Adsorption 4, 113–147 (1998)

On the Optimisation of Periodic Adsorption Processes

S. NILCHAN AND C.C. PANTELIDES
Centre for Process Systems Engineering, Imperial College of Science, Technology and Medicine, London SW7 2BY, United Kingdom
c.pantelides@ic.ac.uk

Abstract. A rigorous mathematical programming based approach to the optimisation of general periodic adsorption processes is presented. Detailed dynamic models taking account of the spatial variation of properties within the adsorption bed(s) are used. The resulting systems of partial differential and algebraic equations are reduced to sets of algebraic constraints by discretisation with respect to both spatial and temporal dimensions. Periodic boundary conditions are imposed to represent directly the "cyclic steady-state" of the system. Additional constraints are introduced to characterise the interactions between multiple beds in the process as well as any relevant design specifications and operating restrictions. The optimal operating and/or design decisions can be determined by solving an optimisation problem with constraints representing a single bed over a single cycle of operation, irrespective of the number of adsorption beds in the process.

Keywords: pressure-swing adsorption, periodic processes, process optimisation, dynamic optimisation

1. Introduction

In recent years, periodic adsorption processes (PAPs) have been finding increasing application as energy-efficient alternatives to other separation techniques (such as cryogenic distillation), and much progress has already been achieved in improving their performance with respect to both the process economics and the attainable purity of the products (see, for instance, Ruthven et al., 1994).

PAPs are intrinsically dynamic, operating in a periodic mode with a fixed cycle time. The periodic excitation is achieved by a regular periodic variation of the upstream and downstream conditions of each bed and the connectivity between multiple beds. Depending on the precise conditions being varied, we may have different classes of PAP (e.g., the well-known "pressure-swing", "temperature-swing" or "concentration-swing"). In any case, after a number of cycles, the bed approaches a "cyclic steady state" (CSS) in which the conditions at the end of each cycle are identical to those at its start.

The performance of PAPs is critically affected by a number of design and operating parameters. The first category includes the size of the bed(s) in the process and the physical characteristics (e.g., particle size) of the adsorbent. On the other hand, important operating parameters include the duration of the various steps and the overall cycle and the pressure and/or temperature levels in each step. The process designer is therefore confronted with an optimisation problem typically aiming to minimise the capital and/or operating costs of the process while ensuring that minimum purity and throughput specifications are met.

In view of the large number of degrees of freedom, a mathematical programming approach to the optimisation of PAPs appears to be highly desirable, but this has to address the intrinsic complexity of the processes being studied, and in particular the complications arising from their periodic nature. This paper is concerned with establishing a rigorous mathematical framework for this task.

In the next section, we present a general mathematical formulation of the problem. In Section 3, this

formulation forms the basis for a critical review of earlier work on the computation of CSS for PAPs, and the description of a novel approach for PAP optimisation. Section 4 presents the application of this new methodology to a simple rapid pressure swing adsorption process (RPSA) comprising a single bed and two steps per cycle. Section 5 considers a more complex process comprising two beds and six operating steps per cycle, with finite rates of intraparticle diffusion. Section 6 concludes with some general remarks on the applicability and the limitations of this work.

2. Mathematical Formulation of the Periodic Adsorption Optimisation Problem

Consider a periodic adsorption process (PAP) comprising one or more identical packed beds, each undergoing a cycle of duration T_c with an operation sequence of N steps. The duration of step k, $(k = 1, \ldots, N)$, is denoted by τ_k and its starting time relative to the start of the cycle by t_k (see Fig. 1). We therefore have the timing relations:

$$\sum_{k=1}^{N} \tau_k = T_c \tag{1}$$

$$t_{k+1} = t_k + \tau_k \quad \forall\, k = 1, \ldots, N \tag{2}$$

where it is understood that $t_1 = 0$ and $t_{N+1} = T_c$.

This section starts with presenting a general mathematical form for models of the operation of a single adsorption bed. Specific examples of such models are presented in Sections 4 and 5. It then proceeds to consider the modelling of the periodic operation of PAPs comprising multiple beds. Finally, it considers some aspects of the corresponding process optimisation problem; these include the decision variables at the disposal of the process designer, the objective function to be optimised and the constraints that the optimal solution has to satisfy.

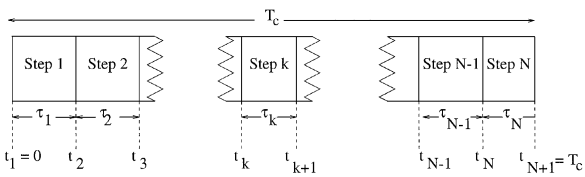

Figure 1. Operating cycle for a bed in a periodic adsorption process.

2.1. Adsorption Bed Modelling

2.1.1. Mathematical Model for Interior of Adsorption Bed. Adsorption beds are intrinsically transient, spatially distributed systems, with the properties in the solid and fluid phases varying over time and one or more spatial dimensions. Usually, the mathematical description of distributed unit operation models leads to partial differential equations (PDEs) expressing the physical laws of conservation of mass, energy and momentum. In addition, algebraic equations (AEs) may be involved in describing relationships between variables, such as the ideal gas law or the adsorption isotherm for gas-solid equilibrium. Overall, the detailed mathematical modelling of the physical phenomena occurring within the adsorption bed leads to mixed sets of partial differential and algebraic equations (PDAEs) of the general form:

$$F(x, x_z, x_{zz}, \dot{x}, y, y_z, v) = 0, \quad \forall z \in (0, L), t \in (0, T_c] \tag{3a}$$

$$\bar{F}(x, x_z, x_{zz}, y, y_z, v) = 0, \quad \forall z \in (0, L), t \in [0, T_c] \tag{3b}$$

where z represents the spatial position in the bed, $\dot{x}$ denotes $\frac{\partial x}{\partial t}$, and F and $\bar{F}$ correspond to differential and algebraic equations respectively. Note that the distinction between the two types of equation is that $\bar{F}(\cdot)$ do not involve time derivatives $\dot{x}$ and also hold at $t = 0$. On the other hand, $F(\cdot)$ do involve $\dot{x}$ and only hold for $t > 0$; at $t = 0$, they are replaced by initial or other temporal conditions (see Section 2.2.1).

For the sake of simplicity of notation, here we assume a single spatial dimension corresponding to the axial position within the bed, i.e., $z \in [0, L]$ where L is the bed length. However, the methodology to be presented is entirely general and can be applied to any number of spatial domains (see, for instance, the example considered in Section 5).

We distinguish two classes of variable in the model (3), namely differential variables $x(z, t)$ and algebraic variables $y(z, t)$, depending on whether or not their partial derivatives with respect to time also appear in the equations. For the models of interest to this paper, the number of differential (algebraic) variables will equal the number of differential (algebraic) equations. In general, the model will also involve spatial derivatives (namely $x_z \equiv \frac{\partial x}{\partial z}$, $x_{zz} \equiv \frac{\partial^2 x}{\partial z^2}$, $y_z \equiv \frac{\partial y}{\partial z}$) arising from convective and dispersive phenomena. It may also

involve certain parameters v that do not vary with either time or spatial position, such as, for instance, the radius of the adsorbent particles.

2.1.2. Spatial Boundary Conditions. The model Eqs. (3a) and (3b) represent the fundamental physics of the adsorption and any other phenomena (e.g., reaction in the fluid and/or solid phases) taking place in the bed. Thus, they are usually the same for all steps of the PAP. What differs from one step to another is the set of boundary conditions at the two ends of the bed, i.e., at $z = 0$ and $z = L$ respectively. These are of the general form:

$$B_L^{(k)}(x(0,t), x_z(0,t), y(0,t), y_z(0,t), u_k(t), v) = 0, \quad \forall t \in (t_k, t_{k+1}], \quad k = 1, \ldots, N \tag{4}$$

$$B_R^{(k)}(x(L,t), x_z(L,t), y(L,t), y_z(L,t), u_k(t), v) = 0, \quad \forall t \in (t_k, t_{k+1}], \quad k = 1, \ldots, N \tag{5}$$

where $B_L^{(k)}(\cdot)$ and $B_R^{(k)}(\cdot)$ represent respectively boundary conditions at the left and right boundaries of the bed over step k. The variables $u_k(t)$ appearing in (4) and (5) represent the feed and product end conditions during step k. These may include the extensive (e.g., flow rate) and intensive (e.g., composition, temperature and pressure) properties of any feed or purge streams, and the downstream pressure for product release or blow down. In general, u_k may vary over the step but they can also be constant.

We note that the PDAE system (3a) and (3b) has been written strictly for the interior of the spatial domain $z \in (0, L)$ and not for the boundaries $z = 0$ and $z = L$. The phenomena taking place at the latter are supposed to be entirely described by the boundary conditions (4) and (5). However, although this is true for models comprising exclusively second-order parabolic partial differential equations, it is not generally correct for all PDAE systems. For instance, an equation of state relating the gas phase density, temperature and pressure is a purely algebraic relation that holds both in the interior of the bed and at its boundaries, without the need for separate boundary conditions. Also, in the absence of dispersive phenomena, Eqs. (3a) and (3b) do not involve the partial derivatives x_{zz} and require boundary conditions at their left boundary ($z = 0$) only.

In order to resolve the above difficulty without complicating the mathematical notation, we accept that any missing "boundary conditions" associated with some of the system equations are, in fact, identical to the equations themselves. This allows us to have the same domain of definition for *all* system equations (3).[1] The obvious consequence is that the number of Eqs. (3), (4) and (5) is the *same* in all three cases, and equals the total number of variables x and y in the model under consideration.

2.1.3. Characterisation of State of Adsorption Bed. A key assumption of our work is that the variation of the differential variables $x(z, t)$ in the interior $z \in (0, L)$ of the bed (i.e., excluding the boundaries) defines completely and uniquely the state of the bed at a given time t. More specifically, we assume that, given:

- $x(z, t), \quad \forall z \in (0, L)$
- $u_k(t)$
- v

Eqs. (3)–(5) allow us to determine unique values for:

- $x(0, t); x(L, t)$
- $y(z, t), \quad \forall z \in [0, L]$
- $\dot{x}(z, t), \quad \forall z \in (0, L)$

This assumption is, in fact, satisfied by most models of adsorption processes used in practice (see examples in Sections 4 and 5).

2.2. *Modelling of Periodic Adsorption Process Operation*

Periodic adsorption processes are intrinsically dynamic, operating in a periodic mode with a given cycle time. The periodic excitation is achieved by a regular periodic variation of the upstream and downstream conditions of each bed and the connectivity between multiple beds. We now turn our attention to the mathematical characterisation of the periodic operation and the interactions among the beds in the process.

2.2.1. Periodicity Conditions. After a sufficiently large number of cycles, the bed approaches a "cyclic steady state" (CSS) in which the conditions at the end of each cycle are identical to those at its start. In terms of the mathematical model presented in Section 2.1, the cyclic steady state can be expressed by:

$$x(z, 0) = x(z, T_c) \quad \forall z \in (0, L) \tag{6}$$

We note that this is sufficient to ensure that *all* variables in the bed (including $y(z,t)$) have reached the cyclic steady state since:

- we have assumed that the values of $x(z,t), z \in (0, L)$, $u(t)$ and v define the state of the bed at time t completely and uniquely (cf. Section 2.1.3);
- due to the periodic nature of the external excitation, $u(t + T_c) = u(t)$;
- parameters v are time-invariant.

2.2.2. Bed Interactions. In addition to the periodicity condition (6), additional constraints are imposed by the interactions among the beds in a given process. Typically, the inputs to a bed during step k of the cycle may involve material being produced by another bed currently undergoing a different step k' of its cycle. For example, in a 2-bed PSA system, some of the product generated during the adsorption step in bed 1 is used to purge bed 2. Of course, when the system reaches the CSS, all adsorption beds are operating under identical conditions with a simple phase difference. Thus, for example, the variation of the composition of the purge fed to bed 1 over the purge step is precisely the same as the variation of the composition of the product stream from the same bed over the product release step. We can, therefore, express the interactions between *different* beds in terms of the variables that have already been introduced to describe the *single* bed operation.

In particular, the input $u_k(t)$ to the bed during a step k may be related to the outputs from the bed during a different step k'. These outputs can normally be expressed in terms of the bed variables $x(z,t)$ and $y(z,t)$ at positions $z = 0$ and/or $z = L$. Mathematically, this leads to a set of constraints of the general form:

$$G^{(kk')}(u_k(t), x(0, t + \delta_{kk'}), y(0, t + \delta_{kk'}), x(L, t + \delta_{kk'}), y(L, t + \delta_{kk'})) = 0, \quad \forall (k, k') \in K, t \in (t_k, t_{k+1}] \tag{7}$$

where K is the set of pairs of steps (k, k') involving such interactions and $\delta_{kk'}$ is the time offset between the two steps k and k':

$$\delta_{kk'} \equiv t_{k'} - t_k \quad \forall (k, k') \in K \tag{8}$$

For constraint (7) to be well posed, any two steps k and k' that interact with each other in this manner must have the same duration. This leads to the additional timing constraints:

$$\tau_k = \tau_{k'} \quad \forall (k, k') \in K \tag{9}$$

This operational feasibility constraint does not result in any loss of generality: if a step k interacts with only part of another step k', then the latter can be considered as two consecutive steps, respectively with and without interaction with step k. Overall, we note that, in constraint (7), as the time t varies over $(t_k, t_{k+1}]$, the shifted time $t + \delta_{kk'}$ varies over $(t_{k'}, t_{k'} + \tau_{k'}]$ which is identical to $(t_{k'}, t_{k'+1}]$.

2.3. Optimisation Decision Variables

The cyclic steady state of a periodic adsorption process implementing a cycle involving a given number N of steps with interactions between given pairs of beds at each step is determined by:

- the PDAE system (3) describing the physical phenomena taking place within each adsorption bed;
- the spatial boundary conditions (4) and (5) describing how each bed interacts with its environment during each step k of the cycle;
- the periodicity condition (6) that ensures cyclic operation;
- the bed interaction constraints (7) that describe the exchange of mass and energy taking place between two beds respectively undergoing steps k and k' of the cycle;
- the cycle timing constraints (1), (2), and (9).

We note that the above constraints, in fact, characterise just a *single* bed. Indeed, the number of beds in the process does not even appear in this formulation. However, as we assume that all beds are identical and undergo the same cycle (albeit with a phase difference), this is sufficient to characterise the cyclic steady state of the entire process.

Of course, in spite of all the above constraints, the process designer is still left with a significant degree of freedom even if both the numbers of steps and beds, and the nature of interactions between beds at each step are fixed. The optimisation decision variables may include:

- the overall cycle time, T_c;
- the duration τ_k of each step k;
- the bed dimension, L;

- the values of the parameters v (e.g., the size of the adsorbent particles);
- the variation of the input variables $u_k(t), \forall t \in (t_k, t_{k+1}]$ over each step k.

In reality, not all of these can be specified completely independently of each other. For instance, the first two items in the above list must satisfy the timing constraints (1) and (9). Also, some of the input variables (e.g., the composition of the purge stream fed to a bed) will implicitly be determined by the bed interaction constraints (7). Other input variables (e.g., the composition of the feed) will be fixed and will not normally be at the disposal of the process designer. We denote the vector of *independent* optimisation decision variables by p:

$$p \equiv \{L, \tau_k, v, \tilde{u}_k(t), t \in (t_k, t_{k+1}], k = 1, \ldots, N\} \tag{10}$$

where $\tilde{u}_k$ denotes the subset of input variables at step k that can be specified independently. In general, the admissible values for these variables will be subject to given lower and upper bounds. We therefore have the additional constraints:

$$p^{\min} \leq p \leq p^{\max} \tag{11}$$

2.4. *Objective Function and Process Performance Specifications*

The periodic adsorption process optimisation may aim to optimise a technical objective (e.g., product purity) subject to various technical and/or economic limitations. Alternatively, it may aim to optimise an economic objective subject to certain minimum performance specifications. In its most general form, it may be expressed in terms of an objective function of the form:

$$\min_p \phi(v, L) + \frac{1}{T_c} \sum_{k=1}^{N} \int_{t_k}^{t_{k+1}} \Psi^{(k)}(u_k(t), x(0,t), y(0,t), x(L,t), y(L,t))\, dt \tag{12}$$

where $\phi(\cdot)$ represents the capital cost depreciation per unit time while $\Psi_k(\cdot)$ is the instantaneous operating cost incurred during step k of the operation of the bed. The operating cost may account for the costs of raw materials, feed pressurisation or heating, as well as that of treating any process exhaust streams prior to disposal. Its functional form may vary from one step to another; in fact, $\Psi^{(k)}$ may be zero for some steps k (e.g., those involving simple bed depressurisation).

The process performance is normally expressed in terms of a relatively small set of variables w (e.g., product purity and recovery) that are functions $W(\cdot)$ of the cumulative bed product(s) over the entire cycle or parts of it:

$$w = W\left(\int_{t_k}^{t_{k+1}} \Omega^{(k)}(u_k(t), x(0,t), y(0,t), x(L,t), y(L,t))\, dt; \quad k = 1, \ldots, N \right) \tag{13}$$

These performance variables may be restricted to lie within given acceptable limits:

$$w^{\min} \leq w \leq w^{\max} \tag{14}$$

reflecting the performance specifications that the process must fulfil.

2.5. *Spatial and Temporal Domain Normalisation*

A complication that arises in the context of the optimisation is that the decision variables p may include the lengths of both the spatial and temporal domains, and these appear only implicitly in many of the equations, determining their domain of definition (e.g., $z \in [0, L]$, $t \in [0, T_c]$). We therefore define a normalised space co-ordinate $\zeta \in [0, 1]$ and a normalised time co-ordinate $\theta_k \in [0, 1]$ within each step k of the cycle as follows:

$$\zeta \equiv \frac{z}{L}; \quad \theta_k \equiv \frac{(t - t_k)}{\tau_k} \quad \forall k = 1, \ldots, N \tag{15}$$

All partial derivatives and integrals can then be expressed in terms of these new independent variables:

$$\frac{\partial}{\partial z} = \frac{1}{L}\frac{\partial}{\partial \zeta}; \quad \frac{\partial^2}{\partial z^2} = \frac{1}{L^2}\frac{\partial^2}{\partial \zeta^2} \tag{16}$$

$$\frac{\partial}{\partial t} = \frac{1}{\tau_k}\frac{\partial}{\partial \theta_k} \quad \forall t \in (t_k, t_{k+1}];$$

$$\int_{t_k}^{t_{k+1}} \pi(t)\, dt = \tau_k \int_0^1 \pi(t_k + \tau_k \theta_k)\, d\theta_k \tag{17}$$

Following these normalisations, the model equations (3a) and (3b) become:

$$F\left(x, \frac{1}{L}x_\zeta, \frac{1}{L^2}x_{\zeta\zeta}, y, \frac{1}{\tau_k}x_{\theta_k}, \frac{1}{L}y_\zeta, v\right) = 0$$
$$\forall \zeta \in (0,1), \theta_k \in (0,1], k = 1, \ldots, N \quad (18a)$$

$$\bar{F}\left(x, \frac{1}{L}x_\zeta, \frac{1}{L^2}x_{\zeta\zeta}, y, \frac{1}{L}y_\zeta, v\right) = 0$$
$$\forall \zeta \in (0,1), \theta_k \in [0,1], k = 1, \ldots, N \quad (18b)$$

and the boundary conditions (4) and (5):

$$B_L^{(k)}\left(x(0,\theta_k), \frac{1}{L}x_\zeta(0,\theta_k), y(0,\theta_k), \frac{1}{L}y_\zeta(0,\theta_k), u_k(t_k + \tau_k\theta_k), v\right) = 0,$$
$$\forall \theta_k \in (0,1], k = 1, \ldots, N \quad (19)$$

and

$$B_R^{(k)}\left(x(1,\theta_k), \frac{1}{L}x_\zeta(1,\theta_k), y(1,\theta_k), \frac{1}{L}y_\zeta(1,\theta_k), u_k(t_k + \tau_k\theta_k), v\right) = 0,$$
$$\forall \theta_k \in (0,1], k = 1, \ldots, N \quad (20)$$

We note that all these equations are now expressed over *fixed* domains of unit length while the quantities L and τ_k appear explicitly in them.

The objective function (12) is transformed to:

$$\min_p \phi(v, L) + \frac{1}{T_c}\sum_{k=1}^{N}\tau_k\int_0^1 \Psi^{(k)}(u_k(t_k + \tau_k\theta_k), x(0,\theta_k), y(0,\theta_k), x(1,\theta_k), y(1,\theta_k))\, d\theta_k \quad (21)$$

The definitions (13) of the performance measures w are similarly transformed.

3. Solution Approaches for the Periodic Adsorption Process Problem

The mathematical formulation presented in the previous section defines a complex time-varying optimisation problem. In fact, most of the earlier literature has been concerned primarily with the solution of the equations (3) to (7) in order to establish the *cyclic steady state* corresponding to a fixed set of the decision variables p defined in Eq. (10).

This section starts with a brief review and critique of earlier work in this area. In particular, the interpretation of this work in terms of the general mathematical formulation of Section 2 allows us to draw some conclusions regarding the relative merits and disadvantages of the various approaches.

We then proceed to propose a new approach to the optimisation of periodic adsorption processes based on the above mathematical formulation.

3.1. *Earlier Approaches to Cyclic Steady State Determination*

The traditional approach to cyclic steady state (CSS) determination has been to apply a Method of Lines methodology (Carver, 1981; Schiesser, 1991) which discretises the spatial dimension(s) to reduce the PDAE system (3) and its boundary conditions (4) and (5) to a set of ordinary differential and algebraic equations (DAEs). The CSS can then be established by starting from a given initial condition and simulating the process operation over a sufficiently large number of cycles. The bed interaction equations (7) are taken into account either exactly (by explicitly including multiple beds in the model), or approximately (by modelling only a single bed, storing its output during step k' and then using it as an input during step k).

Integrating the model equations over a single cycle is equivalent to establishing a mapping $\mathcal{H}(\cdot)$ that, given the spatial profiles of the differential variables x at the start of the cycle, determines the corresponding profiles at the end of the cycle:

$$x(z, T_c) = \mathcal{H}(x(z,0)), \quad \forall z \in (0, L) \quad (22)$$

The traditional approach to determining the periodic steady state can thus be interpreted as an attempt to enforce the periodicity condition (6) through the successive (direct) substitution scheme:

$$x^{[c+1]}(z,0) = \mathcal{H}\left(x^{[c]}(z,0)\right),$$
$$\forall z \in (0, L), c = 1, 2, 3, \ldots \quad (23)$$

where c is the cycle counter. One advantage of such a scheme is that it closely emulates the physical behaviour of the process as it approaches the CSS condition. However, from the mathematical point of view, given the first-order convergence properties of this type of fixed point iteration, it is not surprising that the number of cycles required to reach periodic steady

state may be quite large (often of the order of many hundreds).

More recent work reported in the literature has been considering ways of improving the rate of convergence. For instance, Smith and Westerberg (1991) proposed using a quasi-Newton method for the solution of the equations:

$$x(z,0) - \mathcal{H}(x(z,0)) = 0 \tag{24}$$

The iteration starts with three successive substitution cycles which permit a diagonal approximation to the Jacobian matrix of this system to be constructed. The inverse of this matrix is updated at each subsequent iteration using a least-change secant update formula.

The main advantage of quasi-Newton algorithms is that, theoretically, they attain superlinear convergence rates near the solution. However, since the early 1980s, there has been substantial evidence (see, for instance, Paloschi, 1982) that in most practical applications, satisfactory performance can be achieved only by starting with, and maintaining, a good Jacobian approximation throughout the iterations. In practice, this usually means that the Jacobian must be evaluated using finite differences at the start of the first iteration, and also occasionally at some of the later iterations. However, such an approach would be prohibitively expensive in the PAP context given the size, evaluation cost and complete non-sparsity of the mapping $\mathcal{H}$. In particular, each evaluation of the Jacobian of $\mathcal{H}(\cdot)$ would require $ND + 1$ evaluations of $\mathcal{H}(\cdot)$ where ND is the number of differential variables generated from the discretisation of $x(z,t), z \in (0, L)$. Each evaluation of $\mathcal{H}(\cdot)$ essentially involves the integration of the system equations over a cycle. It is, therefore, doubtful whether such an approach would result in significant savings in computation.

To overcome the above difficulties, Croft and LeVan (1994a) proposed evaluating the Jacobian matrix of (24) by integrating the equations that determine the sensitivities, $\frac{\partial x(z,t)}{\partial x(z,0)}, t \in [0, T_c], z \in [0, L]$, simultaneously with the DAEs that characterise the system behaviour over a cycle. This permits the application of Newton's method to Eq. (24) and therefore guarantees quadratic convergence near the solution provided the sensitivities $\frac{\partial x(z,T_c)}{\partial x(z,0)}, z \in (0, L)$ are computed to sufficient accuracy. The disadvantage is that the computation time is often increased very substantially because of the size and non-sparsity of the sensitivities matrix. For instance, Croft and LeVan (1994a) found that the ratio of the time required for one sensivity evaluation to the time required to do one cycle computation is of the order of $0.4n$ where n is the size of the *discretised* PDAE system (typically of the order of a few hundreds or thousands). Hence, the Newton-type method is competitive only if it results in 2 or 3 orders of magnitude reduction in iterations over the successive substitution method. Furthermore, it is not entirely clear how the bed interactions can be taken into account in formulating these sensitivity equations[2].

A comparison of the above quasi-Newton methods with two simpler schemes, namely the Aitken method for the acceleration of successive substitution iterations and the Muller generalised secant method, has recently been presented by Kvamsdal (1995) who also considered their use in the context of the optimisation of periodic adsorption processes.

3.2. *Overview of Proposed Approach to PAP Optimisation*

It is clear from the above discussion that the efficient computation and optimisation of the CSS of complex PAPs still pose significant challenges. Below, we propose a different approach to these problems. We start with a general overview that aims to establish the key ideas of the approach. Although the latter is conceptually simple, it involves a number of relatively subtle mathematical points. We therefore also provide a detailed example of the application of the approach to a PAP that is of sufficient complexity to illustrate the various relevant issues.

We start by noting that the main complicating factors in the formulation presented in Section 2 are the temporal boundary conditions describing the cyclic steady-state operation of the system and the bed interactions. As will be demonstrated in Section 3.3, the handling of such conditions is facilitated greatly if one simultaneously discretises *both* the spatial domain $z \in [0, L]$ and the temporal domain $t \in [0, T_c]$. This complete discretisation approach immediately reduces the model equations (3), the spatial boundary conditions (4) and (5), and the temporal boundary conditions (6) and (7) to a sparse set of nonlinear algebraic equations of the form:

$$f(\chi, p) = 0 \tag{25}$$

where χ is the vector of unknowns comprising the values of the variables x and y at a finite set of distinct

points on the (z, t) domain, as well as those values of the input variables u_k that are determined by the bed interaction equations (7).

Given the values of the decision variables p (defined in (10)), Eq. (25) can be solved numerically to determine the cyclic steady state directly. The Jacobian of this system is a sparse matrix that can normally be computed analytically, thereby allowing the use of a Newton-type iterative algorithm. Once the CSS is obtained, we can also compute the gradients $\frac{\partial \chi}{\partial p}$ by solving the sparse linear system:

$$\left(\frac{\partial f}{\partial \chi}\right)\frac{\partial \chi}{\partial p} = -\frac{\partial f}{\partial p} \tag{26}$$

where the partial derivatives of f are evaluated at the solution of Eq. (25).

In the context of optimisation, we note that, from the CSS at a given p, we can easily compute the objective function (12) and the performance measures (13). This involves using the discretised variable values χ to approximate the time integrals in these equations in a manner consistent to the discretisation of Eqs. (3) to (5).

Overall, the optimisation problem comprises the objective function (12) the timing constraints (1) and (9), the decision variable bounds (11), and the performance constraints (14). This is a rather small nonlinear programming (NLP) problem expressed entirely in the space of the decision parameters p, and can be solved using standard NLP algorithms (e.g., sequential quadratic programming). The latter will require both the values and the partial derivatives of the objective function and constraints with respect to p. The gradients of (12) and (14) can be expressed in terms of the quantities $\frac{\partial \chi}{\partial p}$ computed by solving (26).

3.3. *A Detailed Illustration of the Proposed Approach*

To illustrate the proposed approach, we consider a pressure swing adsorption process implementing the standard Skarstrom cycle (Skarstrom, 1960). The cycle involves 2 beds and 4 distinct steps, namely feed, blowdown, purge and pressurisation (see Fig. 2).

We focus our attention on Bed 1 in the process, assuming that a model describing the phenomena taking place within it, and the associated spatial boundary conditions at $z = 0$ and $z = L$ for each step of the cycle, is available[3].

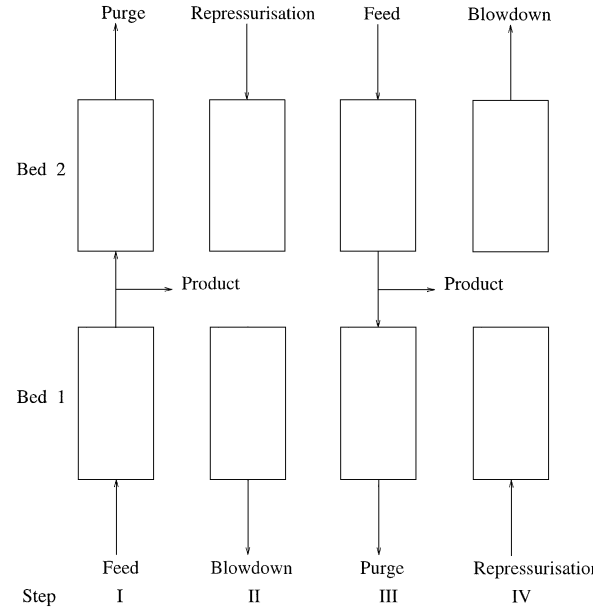

Figure 2. Skarstrom pressure swing adsorption cycle.

3.3.1. Domain Normalisation. We start by normalising the spatial domain $z \in [0, L]$ using a normalised axial position variable $\zeta \in [0, 1]$ (cf. Eq. (15)). We also normalise the temporal domain $t \in [t_k, t_{k+1}]$ within each step $k = 1, \ldots, 4$ of the cycle to obtain a normalised time variable $\theta_k \in [0, 1]$.

The spatial and temporal partial derivatives occurring in the model equations and boundary conditions are modified as indicated by Eqs. (16) and (17). We note that the transformed model equations and boundary conditions over step k of the cycle now explicitly involve the parameters L and τ_k. The transformed Eqs. (18) hold over a domain $\zeta \in (0, 1)$ and $\theta_k \in (0, 1]$. Also, the transformed spatial boundary conditions (19) and (20) hold at $\zeta = 0$ and $\zeta = 1$.

Following the above normalisations, the total length of the time domain for a single cycle is equal to the number of steps N in the cycle, i.e., 4 in this case. The overal effect of the normalisations on the spatial/temporal domain of interest is illustrated in Fig. 3.

We now turn our attention to the temporal boundary conditions that hold at the start of each step k. We recall from Section 2.1.3 that the state of the bed at a given time t is determined by the differential variables $x(z, t)$ in the interior of the spatial domain $z \in (0, L)$. Physical conservation laws imply that the values of these variables (typically representing the holdups of material and energy in the system) are continuous even

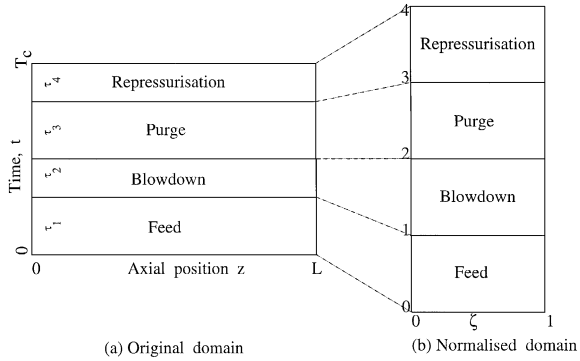

Figure 3. Normalisation of spatial/temporal domain.

at times when the bed is subjected to discontinuities, i.e., when one step of the cycle finishes and the next one starts. This leads to the temporal continuity boundary conditions:

$$x(z, t_k^-) = x(z, t_k^+), \quad \forall z \in (0, L), \quad k = 2, \ldots, N \tag{27}$$

where t_k^- denotes the end of step $k-1$ and t_k^+ the start of step k. In terms of the normalised independent variables, these conditions can be written as:

$$x(\zeta, k^-) = x(\zeta, k^+), \quad \forall \zeta \in (0, 1), \quad k = 1, \ldots, N-1 \tag{28}$$

On the other hand, the periodicity condition (6) can be written as:

$$x(\zeta, 0) = x(\zeta, N), \quad \forall \zeta \in (0, 1) \tag{29}$$

where here $N = 4$ (the number of steps in the cycle).

3.3.2. Domain Discretisation. We now proceed to discretise both the spatial and the temporal normalised domains as shown in Fig. 4. For simplicity, here we adopt a uniform discretisation with the spatial domain being divided into n elements of equal length (nodes $0, \ldots, n$). Also each normalised cycle step is divided into m equal elements, leading to a total of Nm elements (nodes $0, \ldots, Nm$).

We denote the values of the variables x and y at node (i, j) (where i and j correspond to spatial and temporal positions respectively) as X_{ij} and Y_{ij} respectively. Also, the values of the input variables u_k at temporal position j (during step k of the cycle) are denoted by U_{kj}.

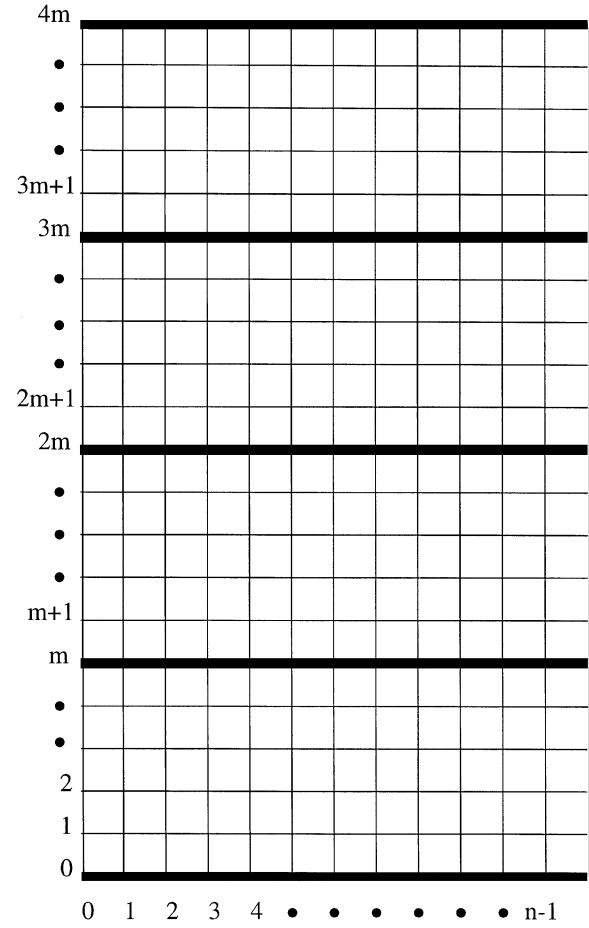

Figure 4. Discretised normalised domain.

We now consider the discretisation of the system equations and boundary conditions. In order to maintain the simplicity of the illustrated example, we apply a centered finite difference approximation to all spatial partial derivatives and a backward finite difference approximation to all temporal ones. The discretised system equations now become:

$$F\left(X_{ij}, \frac{1}{L}\frac{X_{i+1,j} - X_{i-1,j}}{2\delta\zeta}, \frac{1}{L^2}\frac{X_{i+1,j} - 2X_{ij} + X_{i-1,j}}{(\delta\zeta)^2}, \frac{1}{\tau_k}\frac{X_{ij} - X_{i,j-1}}{\delta\theta}, Y_{ij}, \frac{1}{L}\frac{Y_{i+1,j} - Y_{i-1,j}}{2\delta\zeta}, v\right) = 0$$

$$\forall i = 1, \ldots, n-1, \quad j = (k-1)m + 1, \ldots, km, \quad k = 1, \ldots, N \tag{30a}$$

$$\bar{F}\left(X_{ij}, \frac{1}{L}\frac{X_{i+1,j}-X_{i-1,j}}{2\delta\zeta}, \frac{1}{L^2}\frac{X_{i+1,j}-2X_{ij}+X_{i-1,j}}{(\delta\zeta)^2}, Y_{ij}, \frac{1}{L}\frac{Y_{i+1,j}-Y_{i-1,j}}{2\delta\zeta}, v\right)=0,$$
$$\forall i=1,\ldots,n-1, \quad j=0,\ldots,Nm \quad (30b)$$

where $\delta\zeta$ and $\delta\theta$ are the widths of the spatial and temporal discretisation elements respectively. The discretised boundary conditions can be written as:

$$B_L^{(k)}\left(X_{0j}, \frac{1}{L}\frac{X_{1j}-X_{0j}}{\delta\zeta}, Y_{0j}, \frac{1}{L}\frac{Y_{1j}-Y_{0j}}{\delta\zeta}, U_{kj}, v\right)=0,$$
$$\forall j=(k-1)m+1,\ldots,km, \quad k=1,\ldots,N \quad (31)$$

and

$$B_R^{(k)}\left(X_{nj}, \frac{1}{L}\frac{X_{nj}-X_{n-1,j}}{\delta\zeta}, Y_{nj}, \frac{1}{L}\frac{Y_{nj}-Y_{n-1,j}}{\delta\zeta}, U_{kj}, v\right)=0,$$
$$\forall j=(k-1)m+1,\ldots,km, \quad k=1,\ldots,N \quad (32)$$

where U_{kj} are the values of the input variables $u_k(t)$ at the jth temporal node.

We note that the continuity conditions (28) are automatically satisfied in the discretised system since the latter allocates a *single* variable X_{ij} at each node (i, j) on the boundary between steps $k-1$ and k of the cycle (i.e., for $i=1,\ldots,n-1$, $j=(k-1)m$, $k=2,\ldots,N$). However, the periodicity conditions (29) have to be expressed explicitly in terms of the discretised variables. They take the simple form:

$$X_{i0}=X_{i,Nm}, \quad \forall i=1,\ldots,n-1 \quad (33)$$

The discretised boundary conditions (31) and (32) for step k of the cycle concern respectively nodes $(0, j)$ and (n, j) for $j=(k-1)m+1,\ldots,km$. Thus, the boundary conditions that are assumed to hold at $j=km$ are those for step k (rather than $k+1$) of the cycle. This is consistent with the temporal domain of definition (i.e., $t\in(t_k, t_{k+1}]$) of the original boundary conditions (4) and (5).

A problem that arises at this point is that we have not imposed boundary conditions for $j=0$, i.e., for nodes $(0, 0)$ and $(n, 0)$ on Fig. 4. However, at CSS, the start of Step 1 of a cycle coincides with the end of the previous one; therefore, for consistency with the way the boundaries between steps k and $k+1$ are handled for $k\neq N$, we choose to enforce the boundary conditions for the last step $k=N$ also at $j=0$:

$$B_L^{(N)}\left(X_{00}, \frac{1}{L}\frac{X_{10}-X_{00}}{\delta\zeta}, Y_{00}, \frac{1}{L}\frac{Y_{10}-Y_{00}}{\delta\zeta}, U_{N,Nm}, v\right)=0 \quad (34)$$

$$B_R^{(N)}\left(X_{n0}, \frac{1}{L}\frac{X_{n0}-X_{n-1,0}}{\delta\zeta}, Y_{n0}, \frac{1}{L}\frac{Y_{nj}-Y_{n0}}{\delta\zeta}, U_{N,Nm}, v\right)=0 \quad (35)$$

3.3.3. Bed Interactions. So far, we have considered one adsorption bed in isolation. We now proceed to examine the interactions between the two beds in the standard Skarstrom cycle. In particular, we note that the stream being fed to bed 1 during Step III ("purge") of each cycle is part of the product of bed 2. Of course, at CSS, both beds operate identically with a simple phase difference. Hence the *intensive* properties of the input to bed 1 during Step III are determined by the intensive properties of the product of the same bed during Step I. For instance, the compositions (mole fractions) of the two streams are identical while their temperatures and pressures are related via the characteristics of the connecting valve and associated pipework.

Referring to the general formulation of the bed interaction constraints presented in Section 2.2.2, we note that the set K of interacting step pairs (k, k') for this process has a single element:

$$K\equiv\{(3,1)\} \quad (36)$$

and that the interactions take place at the (normally) product end of the bed (i.e., $z=L$). The general interaction constraints (7) can therefore be written as:

$$G^{(3,1)}(u_3(t), x(L, t+\delta_{31}), y(L, t+\delta_{31}))=0, \quad \forall t\in(t_3, t_4] \quad (37)$$

where:

$$\delta_{31}\equiv t_1-t_3=-(\tau_1+\tau_2) \quad (38)$$

Combining (37) and (38), we obtain:

$$G^{(3,1)}(u_3(t), x(L, t-\tau_1-\tau_2), y(L, t-\tau_1-\tau_2)) = 0, \quad \forall t \in (t_3, t_4] \qquad (39)$$

Equation (39) can now be expressed in terms of the discretised variables. In particular, we note that the time domain $t \in (t_3, t_4]$ corresponds to nodes $j = 2m+1, \ldots, 3m$ while the *shifted* time $t-\tau_1-\tau_2$, $t \in (t_3, t_4]$ corresponds to nodes $j = 1, \ldots, m$. We therefore write (39) in discretised form as:

$$G^{(3,1)}(U_{3,2m+j}, X_{nj}, Y_{nj}) = 0, \quad \forall j = 1, \ldots, m \qquad (40)$$

3.3.4. Degree of Freedom Analysis. The discretisation grid illustrated in Fig. 4 involves $(Nm+1)(n+1)$ nodes. Therefore, the number of discretised variables X_{ij} and Y_{ij} is given by:

$$(Nm+1)(n+1)(NX+NY) \qquad (41)$$

where NX and NY are the numbers of differential variables x and algebraic variables y in the original PDAE system (3).

We now proceed to count the discretised equations as shown in Table 1. We note that the total number of equations is equal to the number of variables X_{ij} and Y_{ij}. In fact, these equations can, in principle, be solved for X_{ij} and Y_{ij} if the quantities:

$$L, \{\tau_k, k = 1, \ldots, N\},$$
$$v, \{U_{kj}, j = (k-1)m+1, \ldots, km; k = 1, \ldots, N\}$$

are given[4]. However, we note that the input variables U_{kj} for step $k = 3$ are determined by the bed interaction Eqs. (40). We, therefore, remove these variables from the above set leaving the vector of independent degrees of freedom:

$$p \equiv \{L, \{\tau_k, k = 1, \ldots, N\}, v, \{U_{kj}, j = (k-1)m+1, \ldots, km; k = 1, 2, 4\}\} \qquad (42)$$

For ease of notation, we introduce the vector of unknowns:

$$\chi \equiv \{X_{ij}, Y_{ij}, i = 0, \ldots, n;\ j = 0, \ldots, Nm\} \qquad (43)$$

Finally, the set of equations listed in Table 1, once relations (40) have been used to eliminate the inputs $\{U_{3j},\ j = 2m+1, \ldots, 3m\}$, is denoted by $f(\cdot)$. Overall, we have a system of $(Nm+1)(n+1)(NX+NY)$ nonlinear algebraic equations in χ:

$$f(\chi, p) = 0 \qquad (44)$$

which, of course, is identical to (25).

3.3.5. Process Optimisation Considerations. Since the choice of values of the degrees of freedom p completely determines the process performance via the solution of Eqs. (44), these are also the potential optimisation parameters. However, not all of these are independent: for the standard Skarstrom cycle considered in this section, the bed interactions imply that the durations of the feed and purge steps must be equal (cf., constraints (9)). We therefore have:

$$\tau_1 = \tau_3 \qquad (45)$$

with the overall cycle time, T_c being given by:

$$T_c = \tau_1 + \tau_2 + \tau_3 + \tau_4 \qquad (46)$$

In practice, the decision variables p will also be subject to bounds of the form shown in Eq. (11).

Suppose that the objective of optimisation is to minimise the work of feed compression that is necessary for producing product of a given minimum purity. Since feed compression occurs at the feed end of the bed (i.e., $z = 0$) during Steps I and IV of the cycle, the mean work of compression per cycle is generally given by:

$$\min_p \frac{1}{T_c}\left[\int_{t_1}^{t_2} \Psi(u(t), x(0,t), y(0,t))\,dt + \int_{t_4}^{T_c} \Psi(u(t), x(0,t), y(0,t))\,dt\right] \qquad (47)$$

Table 1. Total number of discretised equations.

Equations	Number
(30a)	$Nm(n-1)NX$
(30b)	$(Nm+1)(n-1)NY$
(31)	$Nm(NX+NY)$
(32)	$Nm(NX+NY)$
(33)	$(n-1)NX$
(34)	$NX+NY$
(35)	$NX+NY$
TOTAL	$(Nm+1)(n+1)(NX+NY)$

where $\Psi(\cdot)$ represents the instantaneous work of compression for given input variables u (e.g., feed pressure and flowrate) and bed inlet conditions $x(0,t)$ and $y(0,t)$.[5] We first express this objective function in terms of the normalised time variable θ in steps $k=1$ and $k=4$ (cf., Eq. (21)):

$$\min_p \frac{1}{T_c}\left[\tau_1 \int_0^1 \Psi(u(\tau_1\theta), x(0,\theta), y(0,\theta))\, d\theta + \tau_4 \int_3^4 \Psi(u(t_4+\tau_4(\theta-3), x(0,\theta), y(0,\theta))\, d\theta\right] \quad (48)$$

We can now approximate the integrals above in terms of the discretised variables U_j, X_{0j} and Y_{0j} using an approximation that is consistent with the method used for partial derivative approximation (see Oh, 1995 for a thorough discussion and derivation of such methods). In general, any such approximation method will replace the integrals with a weighted sum of the values of the integrands at the discretisation nodes. We therefore obtain the discretised objective function:

$$\min_p \frac{1}{T_c}\left[\tau_1 \sum_{j=0}^{m} \lambda_j \Psi(U_{1j}, X_{0j}, Y_{0j}) + \tau_4 \sum_{j=3m}^{4m} \lambda_{j-3m} \Psi(U_{4j}, X_{0j}, Y_{0j})\right] \quad (49)$$

where λ_j, $j=0,\ldots,m$ are appropriate weighting factors determined by the choice of approximation method.

Finally, we turn our attention to the purity constraint mentioned earlier. In practice, this purity will be expressed in terms of the total amount of each component produced by the process during Step I of the cycle, and these amounts will be given by integrals of the form:

$$M_\kappa = \int_0^{\tau_1} \Omega_\kappa(x(L,t), y(L,t))\, dt \quad (50)$$

where $\Omega_\kappa(\cdot)$ would typically be the instantaneously molar flowrate of component κ leaving the bed. Once again, we can first normalise the above integral to:

$$M_\kappa = \tau_1 \int_0^1 \Omega_\kappa(x(1,\theta), y(1,\theta))\, d\theta \quad (51)$$

and then approximate it in terms of the discretised variables X_{nj} and Y_{nj}:

$$M_\kappa \approx \tau_1 \sum_{j=0}^{m} \lambda_j \Omega_\kappa(X_{nj}, Y_{nj}) \quad (52)$$

The minimum purity w^* constraint on a certain component κ^* can then be written simply as:

$$\frac{M_{\kappa^*}}{\sum_\kappa M_\kappa} \geq w^* \quad (53)$$

In conclusion, the optimisation problem comprises the discretised objective function (49), the timing constraints (45) and (46), and the performance constraints (53). The discretised variables X_{ij} and Y_{ij} are *not* treated as optimisation variables since they can always be calculated by solving (25) once the optimiser fixes the values of the decision variables p. This then allows us to calculate the values of the objective function (49) and the constraints (53) for any set of the values of p. In addition to these values, the optimiser may also require the values of the gradients of the objective function and constraints with respect to p. These can be computed using the chain rule of differentiation applied to (49) and (53) with the partial derivatives $\frac{\partial X_{ij}}{\partial p}$ and $\frac{\partial Y_{ij}}{\partial p}$ obtained as indicated by Eq. (26).

The overall computational scheme is as shown in Fig. 5. We note that the optimiser solves a relatively small optimisation problem in the variables p only. The bulk of the computational effort is, in fact, involved in repeatedly solving the large systems of nonlinear algebraic equations (25) to determine χ for given p. A Newton-type iterative scheme may be used for this purpose.

The next two sections consider the application of the technique to two PSA processes.

4. Case Study I: Air Separation Using Rapid Pressure Swing Adsorption

4.1. Introduction

The single-bed rapid pressure swing adsorption (RPSA) process for gas separation was initially proposed for the separation of a nitrogen and methane mixture (Kowler and Kadlec, 1972; Turnock and Kadlec, 1971). Among the pressure swing adsorption processes, the RPSA process offers not only the simplest configuration but also relatively high adsorbate

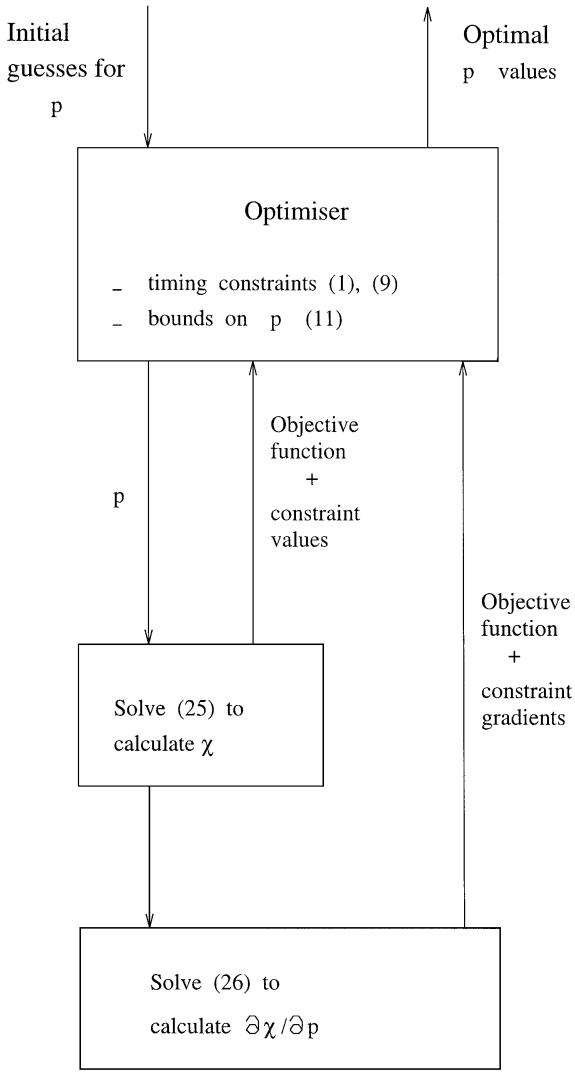

Figure 5. Computational scheme for PAP optimisation.

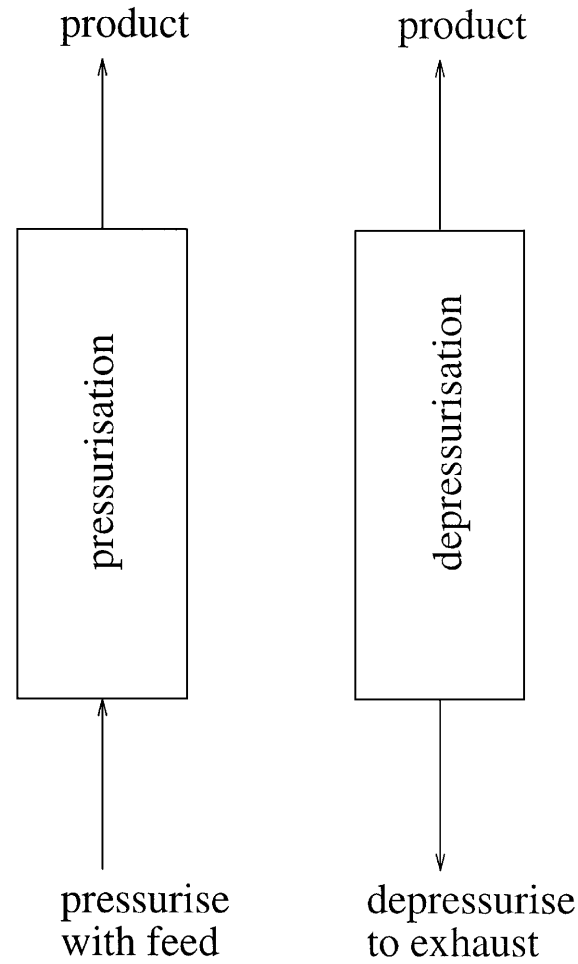

Figure 6. Simple rapid pressure swing adsorption cycle.

productivities for small-scale and low purity separations (Jones and Keller, 1981; Pritchard and Simpson, 1986).

As illustrated in Fig. 6, the simple RPSA cycle comprises two basic steps: pressurisation by feed gas and countercurrent depressurisation with internal purging. The adsorption bed consists of small adsorbent particles with average size between 200–700 μm in diameter, with pressurisation and depressurisation steps of equal durations, normally in the range of 1–5 seconds. The effectiveness of self purging within the RPSA adsorption bed results from a combination of a fast cycle time together with a small particle size leading to steep and periodically varying pressure gradients within the bed. The pressure at the product end is approximately constant over time, which is useful for continuous product release.

The specific process of interest to this case study is air separation using an adsorption bed of zeolite 5A which preferentially adsorbs nitrogen and leaves oxygen in the product stream. The feed pressure considered is in the low pressure range ($\leq$3 bar). Thus the rapid pressure swing adsorption process can be assumed to be isothermal and described by a linear adsorption isotherm. All necessary data were obtained from Alpay (1992).

This section starts with a mathematical model for adsorption in the RPSA process. We then carry out dynamic simulation over a number of cycles to determine the cyclic steady-state in the traditional manner for a set of base conditions. The results obtained are compared

with those from the complete discretisation approach of the type described in Section 3.2. Finally, the RPSA process is optimised with respect to the feed pressure, cycle time, bed length, and adsorbent particle size.

4.2. Mathematical Model for the RPSA Process

4.2.1. Model Assumptions. Our model is based on the following assumptions:

1. The bed operates isothermally.
2. No radial variations occur in the bed.
3. The ideal gas law holds in the fluid phase.
4. All adsorption bed parameters (i.e., bed void fraction, bed bulk density, and particle size) are uniform and constant.
5. Axially dispersed flow takes place in the bed.
6. The axial pressure drop in the bed can be described satisfactorily by Darcy's law.
7. The mass transfer rate is described by a linear driving force model.

4.2.2. Governing Equations. We consider a bed separating a mixture of c components. Based on the assumptions listed in Section 4.2.1, the following modelling equations are derived:

Mass Balance: The component mass balance in the adsorption bed is expressed by:

$$\varepsilon_t \frac{\partial C_i}{\partial t} = -\frac{\partial (v C_i)}{\partial z} + \mathcal{D}_i \frac{\partial^2 C_i}{\partial z^2} - \rho_b \frac{\partial q_i}{\partial t} \quad \forall z \in (0, L), i = 1, \ldots, c \tag{54}$$

where v is the superficial gas velocity, C_i the gas phase concentration of component i, $\mathcal{D}_i$ the axial dispersion coefficient of component i, ρ_b the bed density, q_i the solid phase concentration (in moles of adsorbent per kg of solid), and ε_t the total bed void fraction expressed by:

$$\varepsilon_t = \varepsilon_b + \varepsilon_p (1 - \varepsilon_b) \tag{55}$$

where ε_b represents the bed void fraction and ε_p the particle porosity.

Ideal Gas Law:

$$\frac{P}{RT} = \sum_{i=1}^{c} C_i \quad \forall z \in [0, L] \tag{56}$$

where P is the pressure, T the temperature, and R the universal gas constant.

Pressure Drop Equation: The steady state momentum balance of gas flow at low velocity through a packed bed can be expressed by Darcy's Law:

$$\frac{\partial P}{\partial z} = -\frac{180 \mu v}{d_p^2} \frac{(1 - \varepsilon_b)^2}{\varepsilon_b^3} \quad \forall z \in (0, L] \tag{57}$$

where d_p is the particle diameter and μ the gas viscosity.

Equilibrium Isotherm: We employ the simple linear isotherm:

$$q_i^* = m_i p_i, \quad i = 1, \ldots, c \quad \forall z \in [0, L] \tag{58}$$

where m_i is the adsorption isotherm gradient for component i and p_i the corresponding partial pressure.

Rate of Adsorption: The rate of adsorption is approximated by a linear driving force model (Glueckauf and Coates, 1947):

$$\frac{\partial q_i}{\partial t} = k_i (q_i^* - q_i), \quad i = 1, \ldots, c \quad \forall z \in [0, L] \tag{59}$$

The mass transfer coefficient k_i is given by:

$$k_i = \frac{15}{r_p^2} \frac{\varepsilon_p (1 - \varepsilon_b)}{\rho_b m_i RT} \frac{\varepsilon_p D_p}{\tau_p} \quad i = 1, \ldots, c \tag{60}$$

where r_p is the particle radius ($=d_p/2$) and τ_p the particle tortuosity factor. We assume that the diffusion coefficient D_p is given by (see Ruthven, 1984):

$$\frac{1}{D_p} = \frac{1}{D_k} + \frac{1}{D_m} \tag{61}$$

where D_k and D_m are Knudsen and molecular diffusion coefficients respectively. D_m is proportional to the inverse of the pressure P according to the Chapman-Enskog kinetic theory (see Bird et al., 1960). D_k is taken as a constant.

4.2.3. Boundary Conditions. The governing equations in Section 4.2.2 represent the physical behaviour

of the rapid pressure swing adsorption process in the adsorption bed under all conditions. However, the boundary conditions are different for each of the two operating steps:

At the Feed End: The boundary conditions during the pressurisation step at the feed end of the adsorption bed ($z = 0$) are:

$$v\left(C_i - y_{i,f}\frac{P_f}{RT_f}\right) = D_i\frac{\partial C_i}{\partial z}, \quad i = 1, \ldots, c; \qquad P = P_f \tag{62}$$

where $y_{i,f}$ is the mole fraction of component i in the feed, and T_f and P_f are the feed temperature and pressure respectively.

The boundary conditions during the depressurisation step at the feed end of the adsorption bed $z = 0$ are:

$$\frac{\partial C_i}{\partial z} = 0, \quad i = 1, \ldots, c; \; P = P_w \tag{63}$$

where P_w is the exhaust pressure.

At the Product End: The boundary conditions during both the pressurisation and the depressurisation steps at the product end of the adsorption bed $z = L$ are given by:

$$\frac{\partial C_i}{\partial z} = 0, \quad i = 1, \ldots, c \tag{64}$$

$$v = \frac{Q P_{\text{atm}}}{AP} \tag{65}$$

where Q is the desired product gas volumetric flow rate (corrected to atmospheric pressure P_{atm}), and A the cross sectional area of the adsorption bed.

4.2.4. Performance Measures for the Rapid Pressure Swing Adsorption Process. The separation performance of the rapid pressure swing adsorption process (RPSA) process is assessed on the basis of:

1. The *oxygen product purity*, defined as the ratio between the amount of oxygen collected in the product over a cycle and the total amount of the product:

$$\text{Purity} = \frac{\int_0^{T_c} v(L,t)C_{O_2}(L,t)\,dt}{\sum_{i=1}^{c}\int_0^{T_c} v(L,t)C_i(L,t)\,dt} \tag{66}$$

2. The *oxygen product recovery*, defined as the ratio of the amount of oxygen collected in the product stream over a cycle and the amount of oxygen fed to the bed:

$$\text{Recovery} = \frac{\int_0^{T_c} v(L,t)C_{O_2}(L,t)\,dt}{\int_0^{T_c/2} v(0,t)C_{O_2}(0,t)\,dt} \tag{67}$$

   Note that the integral in the denominator is taken over the first half of the cycle only (i.e., the pressurisation step).
3. The *adsorbent productivity*, defined as the amount of oxygen produced per unit adsorbent weight and time (mol kg^{-1} s^{-1}):

$$\text{Productivity} = \frac{\int_0^{T_c} v(L,t)C_{O_2}(L,t)\,dt}{\rho_b L T_c} \tag{68}$$

4.2.5. Cyclic Steady State Conditions. At cyclic steady state (CSS), the conditions at the end of each cycle are identical to those at its start in both gas and solid phases. Mathematically, the conditions for the CSS can be expressed in terms of the differential variables $C_i(z,t), \forall z \in (0, L)$ (cf., Eq. (54)) and $q_i(z,t), \forall z \in [0, L]$ (cf., Eq. (59)):

$$C_i(z,0) = C_i(z,T_c), \quad \forall z \in (0,L), \; i = 1, \ldots, c \tag{69}$$

$$q_i(z,0) = q_i(z,T_c), \quad \forall z \in [0,L], \; i = 1, \ldots, c \tag{70}$$

At CSS, the molar amount $M_{i,\text{feed}}$ of each component i fed to the bed over a cycle must, in principle, equal the sum of the amounts $M_{i,\text{product}}$ and $M_{i,\text{waste}}$ collected in the product and waste respectively. In practice, this is not exactly true due to the use of numerical discretisation. As a check on the accuracy of the latter, we define the relative mole balance error as:

$$\text{Error}_i = \frac{M_{i,\text{feed}} - M_{i,\text{product}} - M_{i,\text{waste}}}{M_{i,\text{feed}}}, \quad i = 1, \ldots, c \tag{71}$$

4.2.6. Numerical Considerations. The mathematical model of the rapid pressure swing adsorption process is represented by a system of partial differential and algebraic equations (PDAEs). In order to reduce these PDAEs to ordinary differential and algebraic equations (DAEs) in time only, the discretisation method of orthogonal collocation on finite elements (OCFEM) (Carey and Finlayson, 1975; Finlayson, 1980) is applied to the spatial domain.

Table 2. Numerical discretisation characteristics.

Description	Spatial discretisation	Temporal discretisation
Discretisation method	OCFEM	BFDM
Order of approximation	3	2
Number of subdomains	6	30
Collocation points/Grid nodes	19	31

Table 3. Optimisation decision variables for air separation by a rapid pressure swing adsorption process.

Decision variable	Base value	Units	Lower bound	Upper bound
Particle size, d_p	302.5	μm	100	1000
Bed length, L	1.0	m	0.4	1.6
Cycle time, T_c	3.0	s	1.0	5.0
Feed pressure, P_f	2.12	bar	1.0	3.0

One possibility (considered in Section 4.4 below) is simply to integrate the DAEs over time. This is done using the DASOLV code (Jarvis and Pantelides, 1992) with absolute and relative tolerances of 10^{-5}.

The alternative complete discretisation approach requires further discretisation of the temporal domain to reduce the DAEs to systems of nonlinear algebraic equations. A second order backward finite difference method is applied to the temporal domain in this case. The characteristics of the numerical methods used are summarised in Table 2.

The modelling, simulation and optimisation of the RPSA process were carried out using *gPROMS* (*general PROcess Modelling System*), a software package for the modelling and simulation of processes with combined discrete and continuous characteristics. *gPROMS* also allows the direct modelling of systems described by PDAEs; the numerical discretisation is applied automatically to these equations reducing them to DAEs. More information on the package can be found in (Barton and Pantelides, 1994; Oh and Pantelides, 1996).

4.3. *Simulation Conditions*

The RPSA process feed is air at 290 K. The key process design and operating decision variables are listed in Table 3, together with their base values. The table also shows the range of values for each of these variables that will later be considered for the purposes of process optimisation. It should be noted that, throughout this case study, the durations of the pressurisation and depressurisation steps were kept equal to each other (= cycle time/2).

Table 4 shows physical properties of the Zeolite 5A used in air separation as well as other relevant data.

4.4. *Dynamic Simulation of the Rapid Pressure Swing Adsorption Process*

The dynamic simulation of the rapid pressure swing adsorption process is performed to predict both the

Table 4. Data for RPSA process model.

Quantity	Description	Value	Units
d_{pore}	Pore diameter	0.12×10^{-6}	m
D_i	Axial dispersion coefficient ($i = 1, 2$)	10^{-3}	$\text{m}^2\ \text{s}^{-1}$
ε_p	Adsorbent void fraction	0.55	—
ε_b	Bed void fraction	0.35	—
ρ_b	Bed bulk density	800	kg m^{-3}
τ_p	Particle tortuosity factor	3	—
m_i	Adsorption isotherm gradient [N_2,O_2]	$[3.08 \times 10^{-6}$, $1.43 \times 10^{-6}]$	$\text{m}^2\ \text{mol N}^{-1}\ \text{kg}^{-1}$
P_{atm}	Atmospheric pressure	1	bar
P_w	Exhaust pressure	1	bar
Q	Product delivery rate (at atmospheric pressure)	10^{-5}	$\text{m}^3\ \text{s}^{-1}$
μ	Gas viscosity	1.8×10^{-5}	N s m^{-2}

initial transient and the cyclic steady state behaviour. Starting from a given initial condition, the performance of the system is simulated over a large number of cycles until the system reaches the cyclic steady state.

4.4.1. Initial Conditions. The gas phase in the bed is assumed to be initially at the feed (air) composition and atmospheric pressure:

$$C_i(z,0) = y_{i,f}\frac{P_{\text{atm}}}{RT}, \quad \forall z \in (0,L), i = 1,\ldots,c \tag{72}$$

The solid phase is assumed initially to be at equilibrium with the gas. This is conveniently expressed as:

$$\frac{\partial q_i}{\partial t}(z,0) = 0, \quad \forall z \in [0,L], i = 1,\ldots,c \tag{73}$$

which simply states that the rate of adsorption is initially zero everywhere in the bed.

4.4.2. Dynamic Simulation Results. Dynamic simulations were performed for the base case values given in Table 3. The discretised system involves 192 ordinary differential and algebraic equations. Its simulation over 3000 cycles takes approximately 150 minutes on a SUN UltraSPARC workstation. In fact, little change occurs after 2000 cycles.

A number of additional dynamic simulations were performed to determine the effect of the particle size, bed length, feed pressure, and cycle time on the oxygen product purity at CSS. Only one parameter was varied at a time, all others being kept at their base case values.

Figure 7(a) shows the effect of particle size on product purity. Poor performance is observed when the particles are too small (less than 200 μm) or too large (greater than 700 μm).

Figure 7(b) shows the effect of the bed length on product purity. The oxygen product purity decreases when the bed is too short (less than 0.5 m) or too long (more than 1 m).

Figure 7(c) shows that oxygen product purity increases monotonically with feed pressure. On the other hand, Fig. 7(d) indicates that there exists an optimal cycle time for which the oxygen product purity is maximised.

4.5. Direct Cyclic Steady State Determination by Complete Discretisation

Section 4.4 employed the traditional approach to obtaining the cyclic steady state using dynamic simulation. The latter mirrors the behaviour of the real system in that a large number of cycles is required for the system to reach CSS. We now consider the alternative method proposed in Section 3.2 which simultaneously discretises both the spatial and temporal domains in order to determine directly the cyclic steady state. In particular, the temporal domain is now discretised using a second order backward finite difference method on thirty time intervals of equal duration (cf., Table 2). As in the dynamic simulation case, the spatial discretisation is based on third order orthogonal collocation on six finite elements.

4.5.1. Comparative Results. Table 5 presents a comparison of results obtained using the dynamic simulation [DS] and the complete discretisation [CD] approaches to determine the CSS at the base conditions listed in Table 3. It can be seen that generally both approaches produce results that satisfy the overall O_2 mass balance over a cycle to satisfactory accuracy. This provides some evidence that the spatial discretisation used is sufficiently accurate for the purposes of predicting the overall bed performance.

In addition to the major process performance indicators defined in Section 4.2.4, Table 5 also reports the relative difference between each pair of corresponding results. This is calculated as:

$$\%\text{Relative Difference} = \frac{[\text{CD Result}] - [\text{DS Result}]}{[\text{DS Result}]} \times 100 \tag{74}$$

Since the same spatial discretisation was used in both types of approach, this relative difference reflects primarily the error incurred by the discretisation of the temporal domain in the [CD] approach. Of course, the numerical integration of the dynamic model in the [DS] approach is also equivalent to a discretisation of the temporal domain and, therefore, is subject to approximation errors too. However, this integration is carried out at very high accuracy using a variable step length/variable order method.

The relative differences listed in Table 5 indicate excellent agreement between the two approaches. In fact, Nilchan (1997) reports detailed comparative results for

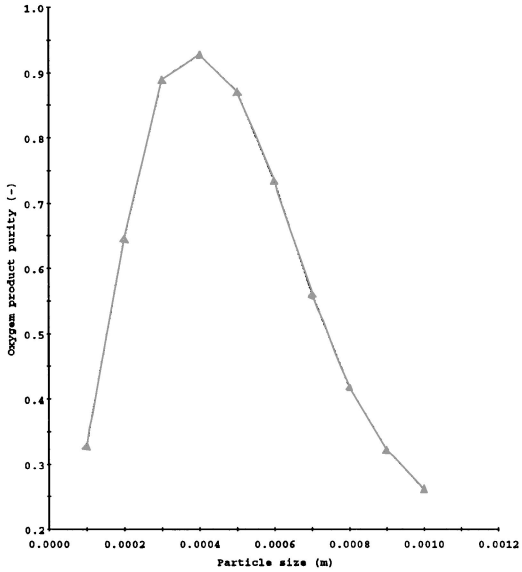

(a) Particle size.

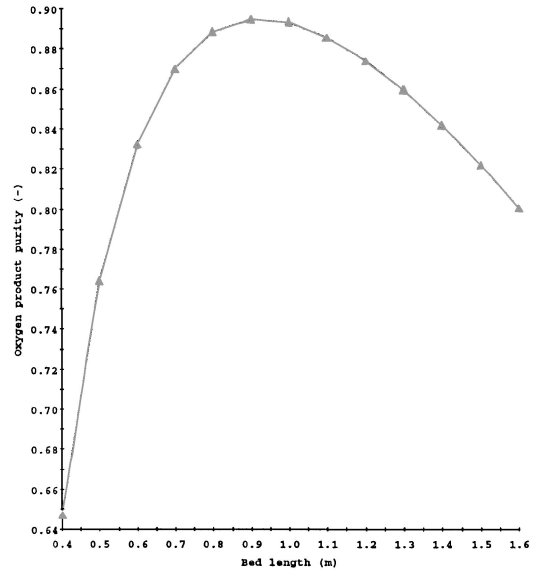

(b) Bed length.

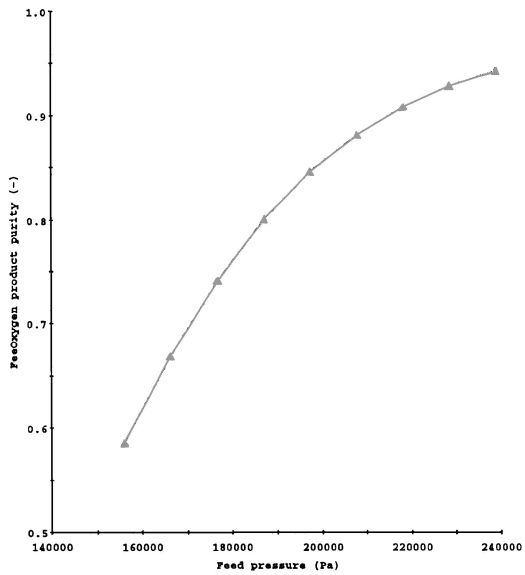

(c) Feed pressure.

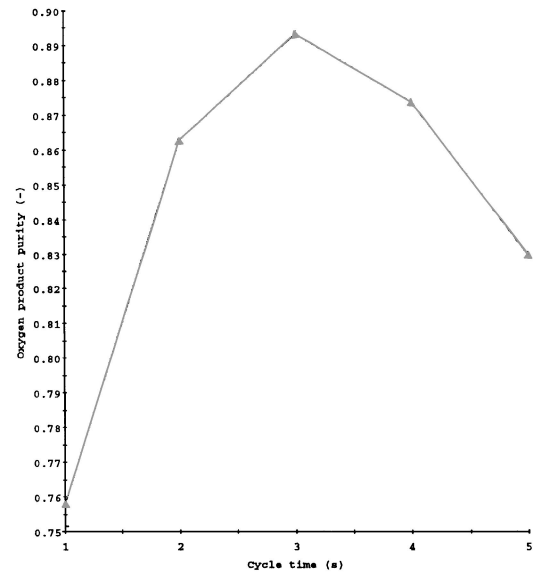

(d) Cycle time.

Figure 7. Effects of parameters on product purity.

Table 5. Dynamic simulation and complete discretisation results for RPSA process at base case conditions.

Performance measure	Dynamic simulation	Complete discretisation	Units	% Relative difference
O_2 purity	89.35	89.18	%	−0.19
O_2 recovery	3.52	3.53	%	0.56
O_2 productivity	2.36×10^{-4}	2.35×10^{-4}	mol kg^{-1} s^{-1}	−0.42
O_2 relative mole balance error	−0.006	−0.003		
Average power requirement	101.45	100.79	W	−0.65
CPU Time (SUN UltraSPARC)	7080	577	s	−91.85

60 runs spanning the entire decision variable ranges indicated in Table 3. She demonstrates that the results generally agree within 1% or better. The most serious exception to this remark was found to occur at very short cycle times, at which discrepancies of up to 10% are observed. This is to be expected: short cycle times correspond to steep temporal variations of the conditions in the bed, which results in higher discretisation errors incurred by the fixed time grid used by the [CD] approach. Clearly, a finer temporal grid is necessary in such cases.

4.5.2. Numerical Efficiency Considerations. The complete discretisation approach results in a system of 3743 nonlinear algebraic equations describing the RPSA behaviour over a single cycle at the cyclic steady state. The Jacobian of the system has 32476 non-zero elements. The equations were solved using a Newton-type iterative method implemented in *gPROMS*; the iterations were initialised with all gas-phase concentrations being set to 8.60 mol m^{-3}, all solid-phase concentrations to 0.07 mol kg^{-1}, all pressures to 10^5 Pa and all velocities to 5×10^{-3} m s^{-1}. Convergence was achieved in 26 iterations.

All complete discretisation [CD] computations were carried out on a SUN UltraSPARC 143 workstation with 256 Mb of memory. The CPU times required for the base case solutions for both the [CD] and the [DS] (over 2000 cycles) approach are also shown in Table 5. These are typical of the more extensive results reported by Nilchan (1997) who found that the [CD] approach is generally an order of magnitude faster than the [DS] one.

Furthermore, it is worth noting that the [CD] approach becomes even more competitive if several related runs are carried out in sequence, with the solution of each one serving as the initial guess for the next. In this case, due to the local quadratic convergence properties of the Newton iteration algorithm used, the solution of all but the first run is obtained in a very small number of iterations. Again, the interested reader is referred to Nilchan (1997) for detailed results illustrating this aspect of the numerical solution.

4.6. Optimisation of the Rapid Pressure Swing Adsorption Process

The performance of the RPSA process is affected by a number of highly interacting design and operating parameters. In this section, the formal mathematical optimisation approach proposed in Section 3.2 is employed to determine the values of these parameters that minimise the power consumed by the feed compression while maintaining a minimum purity of the oxygen.

The theoretical work, W (J mol^{-1}), per mole of gas compressed for a single stage compressor is given by (McCabe et al., 1985):

$$W = \left(\frac{k}{k-1}\right) RT_f \left(\left(\frac{P_f}{P_{\text{atm}}}\right)^{\frac{k-1}{k}} - 1\right) \qquad (75)$$

where k is the ratio of the specific heat capacity at constant pressure to the specific heat capacity at constant volume (for air, $k = 1.4$). The average power requirement is given by:

$$\text{Power} = \frac{W \sum_{i=1}^{c} \int_0^{T_c/2} v(0,t) C_i(0,t)\, dt}{T_c} \qquad (76)$$

The minimum acceptable oxygen product stream purity is set at 89% while the product stream volumetric flowrate Q is held constant at 10^{-5} m^3 s^{-1} (corrected to atmospheric pressure). The cycle time, particle size, bed length, and feed pressure are treated as decision variables with fixed lower and upper bounds, as listed in Table 3.

Table 6. Optimisation results and computational statistics for the RPSA process.

	Decision variable				Process performance		Computational statistics		
Run	d_p (μm)	L (m)	T_c (s)	P_f (bar)	O_2 Purity (%)	Power (W)	CPU time (s)	Workstation	Opt. iter[a]
1	300.9	1.0*	3.0*	2.12*	89.0	100.2	597	UltraSPARC	2
2	302.5*	1.05	3.0*	2.12*	89.0	100.7	538	UltraSPARC	2
3	302.5*	1.0*	5.0†	2.12*	89.1	79.4	533	UltraSPARC	2
4	302.5*	1.0*	3.0*	2.11	89.0	99.6	526	UltraSPARC	2
5	347.8	1.002	4.7	1.99	89.2	75.5	6257	UltraSPARC	11

[a]Number of optimisation iterations.
*Decision variable fixed at corresponding base case value.
†Optimal value of decision variable at upper bound.

We start by performing a number of optimisation runs, in each of which only one of the four decision variables is allowed to vary, all others being held at their base case values. The results obtained and some computational statistics are reported in the first four rows of Table 6.

We then carry out a further optimisation run allowing all four decision variables to be varied simultaneously. The optimal values determined in run 1–4 are used as the starting point for this optimisation. The results obtained are reported in the last row of Table 6. We note that the optimal value of the objective function (75.5 J mol^{-1}) is about 25% smaller than that for the base case (100.8 J mol^{-1}), and considerably smaller than that attained by any one of the single variable optimisation runs 1–4. Moreover, this optimum was obtained within only 11 optimisation iterations taking approximately 100 minutes of CPU time on a desktop workstation.

Of course, since the optimum point was obtained using a complete discretisation approach, the accuracy of the time discretisation method used is a potential concern. We therefore verify the process performance predicted by the optimisation by carrying out a dynamic simulation over 3000 cycles with all decision variables fixed at their optimal values. Table 7 compares the process performance at cyclic steady state as predicted by the dynamic simulation to that predicted by the optimisation run. It is clear that the solution suggested by the optimisation is a true reflection of the process performance and does indeed result in significant improvement over the base case.

Table 7. Verification of RPSA optimisation results via dynamic simulation.

Results	Units	Optimal values predicted by [CD]	Values calculated by [DS]	% Relative difference
Objective function	W	75.45	75.75	0.40
Oxygen purity	%	89.18	89.48	0.33

5. Case Study II: Air Separation for N_2 Enrichment using a Modified PSA Process

The previous section showed how the approach proposed in Section 3.2 can be used for the direct optimisation of a simple PAP involving just a single bed and two operating steps per cycle. In this section, we consider a more complex PAP that involves two interacting beds with six steps per cycle. The mathematical adsorption model employed is also much more complex than that used in Section 4.

5.1. Process Description

The pressure swing adsorption process considered here uses a carbon molecular sieve to produce a nitrogen-rich stream from air. The process exploits the different diffusion rates of oxygen and nitrogen within the pores of the adsorbent particles. In particular, the diffusion of nitrogen in a carbon molecular sieve is much slower than that of oxygen, and therefore nitrogen is separated as a pure product. Thus, the separation is kinetically controlled. This process operates almost isothermally.

A micropore diffusion model is developed to simulate a modified pressure swing adsorption for bulk binary kinetic separation, taking account of both the isotherm non-linearity and the concentration dependence of the micropore diffusivity. The necessary data

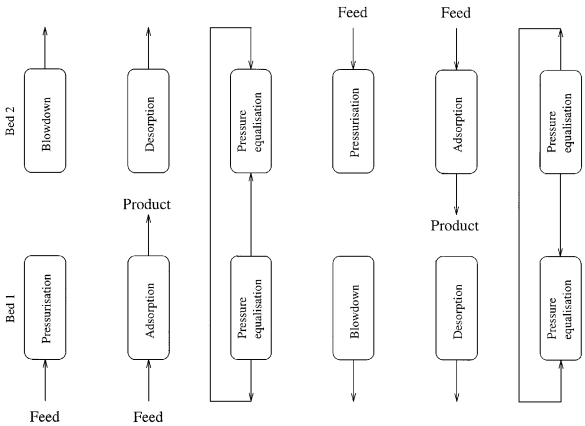

Figure 8. The modified Skarstrom cycle with pressure equalisation and desorption steps.

were taken from Hassan et al. (1986) and Farooq and Ruthven (1991).

The process employs a modified Skarstrom cycle which performs six operating steps in two adsorption beds (see Fig. 8). Two pressure equalisation steps were added to the original Skarstrom cycle (see Fig. 2) with the replacement of the purge step by a desorption step. The advantage of eliminating the purge step is that the product recovery is enhanced (see Hassan et al., 1987). The pressure equalisation steps exploit the blowdown of the high pressure bed to pressurise the low pressure one. This reduces the amount of energy required for the pressurisation.

The modified Skarstrom cycle comprises the following steps:

1. *Pressurisation.* Bed 1 is pressurised with the feed gas at the feed end of the bed while the product end is closed. At the same time, bed 2 is blown down to the lower operating pressure (usually atmospheric).
2. *Adsorption.* The high pressure feed is fed to bed 1 where the faster diffusing component (O_2) is adsorbed onto the solid particles, leaving the slower diffusing component (N_2) as a product in the exit stream. The product end is opened and the N_2 is withdrawn. At the same time, bed 2 is desorbed.
3. *First Pressure Equalisation.* Both feed and product ends of the two beds are connected to each other to ensure a rapid gas transfer.
4. *Blowdown.* The pressure in bed 1 is reduced to the low pressure by releasing gas at the feed end while the product end is closed. During this time, bed 2 is pressurised with feed gas at the feed end.
5. *Desorption.* Bed 1 is disconnected for a while with the feed end open and the product end is closed. During this time, the small amount of the slower diffusing component (N_2) which has been adsorbed during the adsorption step, desorbs. At the same time, bed 2 is used for product generation.
6. *Second Pressure Equalisation.* This is the same as the first pressure equalisation with the flows reversed.

Typical durations for the adsorption and desorption operating steps are 60 s. The other four steps are much shorter, typically 2 s.

5.2. Mathematical Model

For a kinetically controlled pressure swing adsorption process such as the one considered here, a proper representation of mass transfer kinetics is essential for accurate prediction of the system performance over a relatively wide range of conditions. Thus, instead of characterising the adsorption rate by a simple linear driving force model (cf., Section 4.2.2), here we employ a more realistic representation which describes the diffusion of the adsorbed components within the micropores of the solid particles. The concentration dependence of the diffusivity within the micropores is also accounted for. An equation describing the mass transfer across the external film of the adsorbed phase provides the necessary link to the gas phase.

5.2.1. Model Assumptions. The main assumptions for our mathematical model are as follows:

1. The process operates isothermally.
2. The pressure drop along the adsorption bed is determined by Darcy's law.
3. The ideal gas law applies to the fluid phase.
4. The equilibrium relationship for both components is represented by a binary Langmuir isotherm with the same saturation capacity for both adsorbates.
5. The flow pattern is described by the axial dispersed plug flow model.
6. The adsorbent consists of uniform microporous spheres. Any macropore diffusional resistance is neglected. The controlling diffusional resistance in a kinetic separation is in the micropores of the adsorbent.
7. The gradient of chemical potential is taken as the driving force for micropore diffusion with a constant intrinsic mobility. This leads to a Fickian diffusion

phenomenon in which the diffusivity is a function of the adsorbed phase concentrations.
8. The fluid and solid phases are linked through an external film resistance.
9. No variation of conditions occurs in the radial direction within the bed.

5.2.2. Governing Equations. For ease of reference, the symbols used in our model are listed in Table 8.

Gas Phase Mass Balance: The mass balance for each component within the gas phase is given by:

$$\frac{\partial C_i}{\partial t} = D_L \frac{\partial^2 C_i}{\partial z^2} - \frac{\partial (vC_i)}{\partial z} - \frac{1-\varepsilon}{\varepsilon}\frac{3}{R_p} k_f \left(C_i - C_{R_p,i}\right), \quad \forall z \in (0, L), i = 1, \ldots, c \quad (77)$$

Equilibrium Isotherm: The equilibrium concentration in the gas phase $C_{R_p,i}$ is related to the concentration $q_{R_p,i}$ on the surface of the solid through the equilibrium isotherm:

$$\frac{q_{R_p,i}}{q_{s,i}} = \frac{b_i C_{R_p,i}}{1 + \sum_{j=1}^{c} b_j C_{R_p,j}}, \quad \forall z \in [0, L], \; i = 1, \ldots, c \quad (78)$$

Ideal Gas Law: Ideal gas behaviour is assumed:

$$\sum_{i=1}^{c} C_i = \frac{P}{RT}, \quad \forall z \in [0, L] \quad (79)$$

Pressure Drop Equation: The pressure drop along the axial direction of the adsorbent bed is described by Darcy's law:

$$\frac{\partial P}{\partial z} = -\frac{180 \mu v}{(2R_p)^2} \frac{(1-\varepsilon)^2}{\varepsilon^3} \quad \forall z \in [0, L] \quad (80)$$

Adsorbed Phase Mass Balance: The rate of adsorption within a particle is given by the standard diffusion equation in spherical coordinates:

$$\frac{\partial q_i}{\partial t} = \frac{1}{r^2}\left[\frac{\partial}{\partial r}\left(D_i r^2 \frac{\partial q_i}{\partial r}\right)\right], \quad \forall r \in (0, R_p), \; z \in [0, L], i = 1, \ldots, c \quad (81)$$

We note that the adsorbed phase concentrations q_i are functions of both axial position z within the bed and radial position r within the particle, as well as time t. In particular, the solid surface concentrations $q_{R_p,i}(z, t)$ are equivalent to $q_i(z, R_p, t)$.

The following expressions for the micropore diffusivity D_i $(i = O_2, N_2)$ in a binary Langmuir system with constant intrinsic mobilities (D_{0,O_2}, D_{0,N_2}) have been suggested by Habgood (1958) and Round et al. (1966):

$$D_{O_2} = \frac{D_{0,O_2}}{1 - \theta_{O_2} - \theta_{N_2}}\left[\left(1 - \theta_{N_2}\right) + \theta_{O_2}\frac{\partial q_{N_2}/\partial r}{\partial q_{O_2}/\partial r}\right], \quad \forall r \in [0, R_p], z \in [0, L] \quad (82)$$

$$D_{N_2} = \frac{D_{0,N_2}}{1 - \theta_{N_2} - \theta_{O_2}}\left[\left(1 - \theta_{O_2}\right) + \theta_{N_2}\frac{\partial q_{O_2}/\partial r}{\partial q_{N_2}/\partial r}\right], \quad \forall r \in [0, R_p], z \in [0, L] \quad (83)$$

where $\theta_i \equiv q_i / q_{s,i}$.

The appropriate forms for the diffusion equations are obtained by substituting these expressions in the particle balance equation (81). Thus, the mass balances for the two components in the adsorbed phase can be expressed as:

$$\frac{\partial q_{O_2}}{\partial t} = \frac{D_{0,O_2}}{1 - \theta_{O_2} - \theta_{N_2}}\left[(1 - \theta_{N_2})\left(\frac{\partial^2 q_{O_2}}{\partial r^2} + \frac{2}{r}\frac{\partial q_{O_2}}{\partial r}\right) + \theta_{O_2}\left(\frac{\partial^2 q_{N_2}}{\partial r^2} + \frac{2}{r}\frac{\partial q_{N_2}}{\partial r}\right)\right] + \frac{D_{0,O_2}}{(1 - \theta_{O_2} - \theta_{N_2})^2} \times \left[(1 - \theta_{N_2})\frac{\partial \theta_{O_2}}{\partial r} + \theta_{O_2}\frac{\partial \theta_{N_2}}{\partial r}\right]\left(\frac{\partial q_{O_2}}{\partial r} + \frac{\partial q_{N_2}}{\partial r}\right), \quad \forall z \in [0, L], r \in (0, R_p) \quad (84)$$

$$\frac{\partial q_{N_2}}{\partial t} = \frac{D_{0,N_2}}{1 - \theta_{O_2} - \theta_{N_2}}\left[(1 - \theta_{O_2})\left(\frac{\partial^2 q_{N_2}}{\partial r^2} + \frac{2}{r}\frac{\partial q_{N_2}}{\partial r}\right) + \theta_{N_2}\left(\frac{\partial^2 q_{O_2}}{\partial r^2} + \frac{2}{r}\frac{\partial q_{O_2}}{\partial r}\right)\right] + \frac{D_{0,N_2}}{(1 - \theta_{O_2} - \theta_{N_2})^2} \times \left[(1 - \theta_{O_2})\frac{\partial \theta_{N_2}}{\partial r} + \theta_{N_2}\frac{\partial \theta_{O_2}}{\partial r}\right]\left(\frac{\partial q_{N_2}}{\partial r} + \frac{\partial q_{O_2}}{\partial r}\right), \quad \forall z \in [0, L], r \in (0, R_p) \quad (85)$$

Note that, in the derivation of these expressions, it is assumed that the saturation limit is the same for both components $(q_{O_2,s} = q_{N_2,s})$: if this is not true, the expressions will contain additional terms (Farooq and Ruthven, 1991).

Table 8. Summary of symbols used in modified pressure swing adsorption model.

Symbol	Quantity described	Units
b_i	Langmuir constant for component i	$m^3\ mol^{-1}$
c	Number of components	—
C_i	Gas phase concentration of component i	$mol\ m^{-3}$
$C_{R_p,i}$	Equilibrium concentration of component i in external film	$mol\ m^{-3}$
C_v	Valve coefficient	$m\ s\ mol^{1/2}\ K^{1/2}\ kg^{-1/2}$
D_L	Axial dispersion coefficient	$m^2\ s^{-1}$
D_i	Micropore diffusivity of component i	$m^2\ s^{-1}$
$D_{0,i}$	Intrinsic mobility of component i in microparticle	$m^2\ s^{-1}$
k_f	External film mass transfer coefficient	$m\ s^{-1}$
L	Length of adsorbent bed	m
MW_i	Molecular weight of component i	$kg\ mol^{-1}$
$\bar{\dot{n}}$	Average molar flow rate	$mol\ s^{-1}$
P	Gas phase pressure	Pa
P_f	Feed pressure	Pa
q_i	Adsorbed phase concentration of component i	$mol\ m^{-3}$
$q_{R_p,i}$	Adsorbed phase concentration of component i on surface of particle	$mol\ m^{-3}$
$q_{s,i}$	Saturation limit of component i	$mol\ m^{-3}$
r	Radial distance within particle	m
R	Universal gas constant	$J\ mol^{-1}\ K^{-1}$
R_b	Bed radius	m
R_p	Particle radius	m
t	Time	s
t_0	Starting time of the pressurization step	s
t_{sa}	Starting time of the adsorption step	s
t_{ea}	End time of the adsorption step	s
t_{sb}	Start time of the blowdown step	s
t_{ed}	End time of the desorption step	s
T	Operating temperature	K
T_c	Cycle time	s
v	Fluid velocity	$m\ s^{-1}$
$y_{i,f}$	Molar gas fraction of component i in feed stream	—
z	Axial distance	m
ε	Bed void fraction	—
θ_i	Normalized adsorbed phase concentration of component i ($\equiv q_i/q_{s,i}$)	—
μ	Gas viscosity	Pa s

5.2.3. Gas Phase Boundary Conditions. The precise form of these boundary conditions depends on the cycle step performed. If a gas stream is entering or leaving the bed during a cycle step, the velocity is given by the valve equation (see Chou and Huang, 1994a, 1994b):

$$v = \begin{cases} C_v \frac{R}{\varepsilon\pi R_b^2}\sqrt{\frac{T}{\sum_{i=1}^{c} y_i MW_i}}\, 1.1792486\sqrt{\frac{P_{\text{upper}}^2 - P_{\text{lower}}^2}{P^2}} \\ \qquad\qquad \text{if } P_{\text{lower}} > 0.53 P_{\text{upper}} \\ C_v \frac{R}{\varepsilon\pi R_b^2}\sqrt{\frac{T}{\sum_{i=1}^{c} y_i MW_i}}\, \frac{P_{\text{upper}}}{P} \\ \qquad\qquad \text{if } P_{\text{lower}} \le 0.53 P_{\text{upper}} \end{cases} \tag{86}$$

Here, P is the pressure at the end of the adsorbent bed. P_{upper} and P_{lower} are the pressures on either side of the valve such that the former is always larger than the latter.

Incoming Gas Stream: The concentration of each component at the bed inlet is determined by the Danckwert's boundary condition:

$$v\left(C_i - y_{i,f}\frac{P}{RT}\right) = D_L \frac{\partial C_i}{\partial z}, \quad i = 1, \ldots, c \tag{87}$$

During the adsorption step, $y_{i,f}$ is the mole fraction of component i in the fresh feed. On the other hand, for the pressure equalisation step, $y_{i,f}$ is, in fact, the mole fraction of component i in the gas leaving the high pressure bed. This can be related to the concentrations at the end of that bed via:

$$y_{i,f} = \frac{C_{i,HP} RT}{P_{HP}}, \quad i = 1, \ldots, c \tag{88}$$

The velocity of the incoming gas stream is determined by the valve equation given above.

Outgoing Gas Stream: The axial gradient of the concentration of each component at the end where a gas stream is leaving the bed is zero:

$$\frac{\partial c_i}{\partial z} = 0, \quad i = 1, \ldots, c \tag{89}$$

The velocity of an outgoing gas stream is determined by the valve equation given above.

Closed Bed End: At a closed bed end, the axial gradient of the concentration of each component is zero:

$$\frac{\partial c_i}{\partial z} = 0, \quad i = 1, \ldots, c \tag{90}$$

The velocity at a closed bed end is also zero:

$$v = 0$$

5.2.4. Adsorbed Phase Boundary Conditions. Boundary conditions are needed to describe the conditions at the centre and on the surface of the adsorbent particle.

Centre of Adsorbent Particle: The usual radial symmetry condition at $r = 0$ leads to:

$$\frac{\partial q_i}{\partial r} = 0, \quad \forall z \in [0, L], \quad i = 1, \ldots, c \tag{91}$$

Surface of the Adsorbent Particle: On the surface of the adsorbent particle ($r = R_p$), the mass transfer by diffusion to the surface must equal the mass transfer rate across the external film:

$$D_i \frac{\partial q_i}{\partial r} = k_f (C_i - C_{R_p,i}), \quad \forall z \in [0, L], \quad i = 1, \ldots, c \tag{92}$$

where D_i are given by expressions (82) and (83).

5.2.5. Performance Measures for the Modified Skarstrom Cycle Process. Additional equations are needed to calculate variables which are useful in analysing the performance of the process:

1. The *oxygen impurity* is defined as the mole fraction of oxygen in the product averaged over the adsorption step at cyclic steady state:

$$\bar{y}_{\text{O}_2,\text{product}} = \frac{1}{1 + \frac{\int_{t_{sa}}^{t_{ea}} C_{\text{N}_2}(L,t)v(L,t)dt}{\int_{t_{sa}}^{t_{ea}} C_{\text{O}_2}(L,t)v(L,t)dt}} \tag{93}$$

2. The *product recovery* is defined as the ratio of nitrogen in the product to nitrogen in feed:

$$\text{rec}_{\text{N}_2} = \frac{\int_{t_{sa}}^{t_{ea}} C_{\text{N}_2}(L,t)v(L,t)\,dt}{\int_{t_0}^{t_{ea}} C_{\text{N}_2}(0,t)v(0,t)\,dt} \tag{94}$$

3. The *average production rate* achieved by each column is the molar flow rate at the product end of the adsorbent bed during the adsorption step divided by the entire cycle time, T_c:

$$\bar{\dot{n}}_{\text{product}} = \frac{1}{T_c}\frac{\varepsilon\pi R_b^2}{RT}\int_{t_{sa}}^{t_{ea}} v(L,t)P(L,t)\,dt \tag{95}$$

4. The *feed rate* for each column is the molar flow at the feed end of the bed during the pressurisation and adsorption step averaged over the entire cycle time, T_c:

$$\bar{n}_{\text{feed}} = \frac{1}{T_c}\frac{\varepsilon\pi R_b^2}{RT}\int_{t_0}^{t_{ea}} v(0,t)P(0,t)\,dt \qquad (96)$$

5. The *average power requirement* over a cycle is given by:

$$\text{Power} = \frac{W\bar{n}_{\text{feed}}}{T_c} \qquad (97)$$

where W is the work of compression per mole of feed given by Eq. (75).

5.2.6. Cyclic Steady State Conditions. The periodicity conditions for the CSS can be expressed in terms of the differential variables $C_i(z,t), \forall z \in (0,L)$ (cf., Eq. (77)) and $q_i(z,r,t), \forall z \in [0,L], r \in (0,R_p)$ (cf., Eq. (81)):

$$C_i(z,0) = C_i(z,T_c), \quad \forall z \in (0,L), \quad i = 1,\ldots,c \qquad (98)$$

$$q_i(z,r,0) = q_i(z,r,T_c), \quad \forall z \in [0,L], \quad r \in (0,R_p), i = 1,\ldots,c \qquad (99)$$

5.2.7. Numerical Considerations. The mathematical model of the PSA process considered in this section involves a system of partial differential and algebraic equations (PDAEs) in time and two spatial dimensions.

A third order orthogonal collocation method on finite elements was used for the discretisation of both the axial and the radial domains. The axial domain was divided into four equal elements for this purpose. On the other hand, the entire radial domain was represented by a single element. This was adequate given the fact that only diffusive mass transfer takes place in this domain and, consequently, steep radial concentration fronts are unlikely to form.

The discretisation of the two space dimensions results in a system of 794 ordinary differential and algebraic equations. As described in Section 5.4 below, these can be integrated directly; this was done using the DASOLV code (Jarvis and Pantelides, 1992) with absolute and relative tolerances of 10^{-5}.

The alternative complete discretisation approach requires further discretisation of the temporal domain. A first order backward finite difference method using 72 intervals of equal length is used for this purpose.

As in the case of the RPSA process considered earlier, the model was implemented, simulated and optimised using the *gPROMS* software (cf., Section 4.2.6).

Table 9. Range of investigation of design parameters and base case values.

Decision variable	Units	Investigation range	Base case value
Feed pressure	bar	2.0–6.0	3.0
Bed length	m	0.1–0.5	0.35
Pressurisation time	s	1.0–10.0	2.0
Adsorption time	s	30.0–100.0	60.0
Pressure equilisation time	s	1.0–10.0	2.0
Blowdown time	s	1.0–10.0	2.0
Desorption time	s	30.0–100.0	60.0

5.3. Simulation Conditions

The PSA process feed is air at 298 K. The key process design and operating decision variables are listed in Table 9, together with their base values. The table also shows the range of values for each of these variables that will later be considered for the purposes of process optimisation.

Table 10 shows physical properties of the adsorbent and other relevant data.

5.4. Dynamic Simulation of the Modified Skarstrom Cycle Process

As with the previous case study, we start by carrying out dynamic simulation over a number of cycles in order to establish the CSS in the traditional manner. It should be noted that the model that we used for this purpose incorporates *two* beds and models rigorously all interactions between them.

5.4.1. Initial Conditions. The gas phase in the two beds is assumed to be initially air at 1 bar and 3 bar respectively. The adsorbed phase is assumed to be in equilibrium with the gas phase (cf., Eq. (73)).

5.4.2. Base Case Dynamic Simulation Results. Figure 9 shows some aspects of the approach of the 2-bed PSA system to the CSS. The amount of oxygen impurity in the product, recovery of nitrogen, production

Table 10. Data for modified Skarstrom cycle process model.

Symbol	Description	Value	Units
b_{O_2}	Langmuir constant for O_2	3.5×10^{-3}	$m^3\ mol^{-1}$
b_{N_2}	Langmuir constant for N_2	3.37×10^{-3}	$m^3\ mol^{-1}$
C_{v_1}	Valve coefficient at the feed end during pressurisation	4×10^{-8}	$m\ s\ mol^{1/2}\ K^{1/2}\ kg^{-1/2}$
C_{v_2}	Valve coefficient at the product end during adsorption	6.3×10^{-9}	$m\ s\ mol^{1/2}\ K^{1/2}\ kg^{-1/2}$
C_{v_3}	Valve coefficient at the product end during pressure equalisation	3×10^{-8}	$m\ s\ mol^{1/2}\ K^{1/2}\ kg^{-1/2}$
C_{v_4}	Valve coefficient at the feed end during blowdown	9×10^{-8}	$m\ s\ mol^{1/2}\ K^{1/2}\ kg^{-1/2}$
C_{v_5}	Valve coefficient at the feed end during desorption	7.5×10^{-9}	$m\ s\ mol^{1/2}\ K^{1/2}\ kg^{-1/2}$
D_L	Axial dispersion coefficient	4.9×10^{-6}	$m^2\ s^{-1}$
μ	Gas viscosity	1.8×10^{-5}	Pa s
D_{0,O_2}	Micropore diffusivity of oxygen	6.75×10^{-8}	$m^2\ s^{-1}$
D_{0,N_2}	Micropore diffusivity of nitrogen	1.475×10^{-9}	$m^2\ s^{-1}$
k_f	Mass transfer coefficient in external film	0.02	$m\ s^{-1}$
MW_{O_2}	Molecular weight of O_2	0.032	$kg\ mol^{-1}$
MW_{N_2}	Molecular weight of N_2	0.028	$kg\ mol^{-1}$
P_{atm}	Exhaust pressure	1×10^5	Pa
q_{s,O_2}	Saturation constant for O_2	2.64×10^3	$mol\ m^{-3}$
q_{s,N_2}	Saturation constant for N_2	2.64×10^3	$mol\ m^{-3}$
R_b	Bed radius	0.0175	m
R_p	Particle radius	0.003175	m
ε	Bed void fraction	0.4	—
R	Universal gas constant	8.314	$J\ mol^{-1}\ K^{-1}$
T	Temperature	298.15	K
$y_{O_2,feed}$	Mole fraction of O_2 in feed	0.21	—
$y_{N_2,feed}$	Mole fraction of N_2 in feed	0.79	—

rate and feed rate are monitored during the first 7680 seconds (60 cycles) of the simulation. It is clear that this time is sufficient for the system to reach CSS.

Figure 10 shows the pressure variation within the first bed over a cycle at CSS. Results are shown for three positions, namely $z = 0$, $z = L/2$ and $z = L$. It can be seen that no significant pressure drop occurs within this bed. On the other hand, it is interesting to note that the desorption of material out of the adsorbent particles into the gas phase causes the pressure to increase during the initial part of the desorption step (i.e., the period from 66 s to 126 s). Once this gas has left the bed at the open feed end, then the pressure starts dropping again.

Figure 11 shows the time variation of the nitrogen mole fraction at five different axial positions over a cycle at CSS. The difference in the mole fraction during high pressure and low pressure steps can easily be seen. The drop in nitrogen mole fraction is caused by the saturation of the adsorbent particles. The fast changes of the mole fraction at the end of the cycle are a consequence of the pressure equalisation introducing gas of a completely different mole fraction into the bed.

Figure 12 shows the time variation of the oxygen concentration within the adsorbed phase at $z = L/4$. The radial positions studied (0, $0.2113R_p$, $0.7887R_p$ and R_p) correspond to the positions of the collocation points. As can be seen, the concentration increases during the high pressure steps and decreases during the low pressure steps.

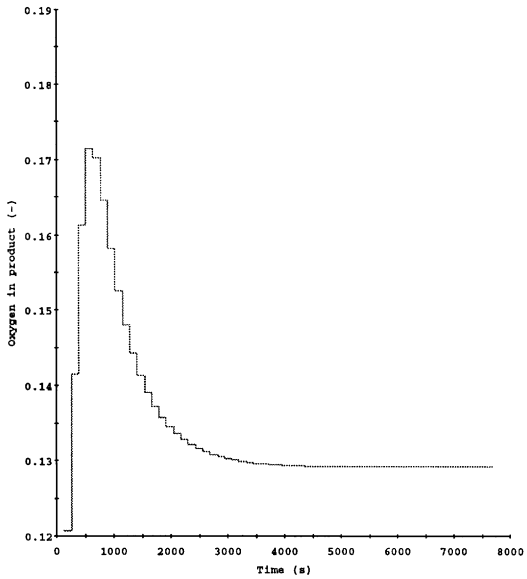

(a) Mole fraction of oxygen in product

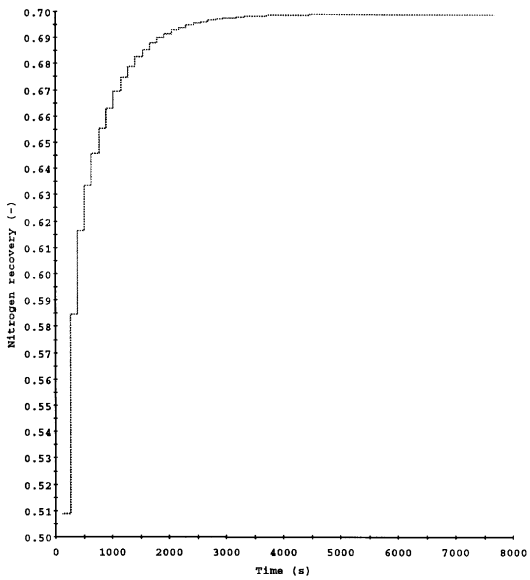

(b) Nitrogen recovery

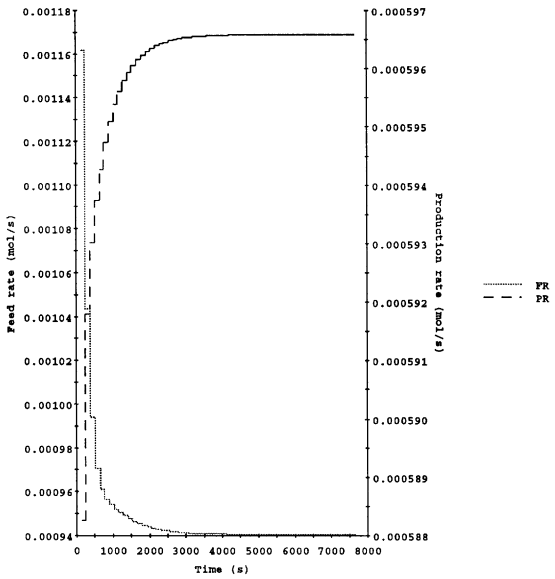

(c) Feed rate (FR) and production rate (PR)

Figure 9. Approach of modified Skarstrom cycle process to CSS at base case conditions.

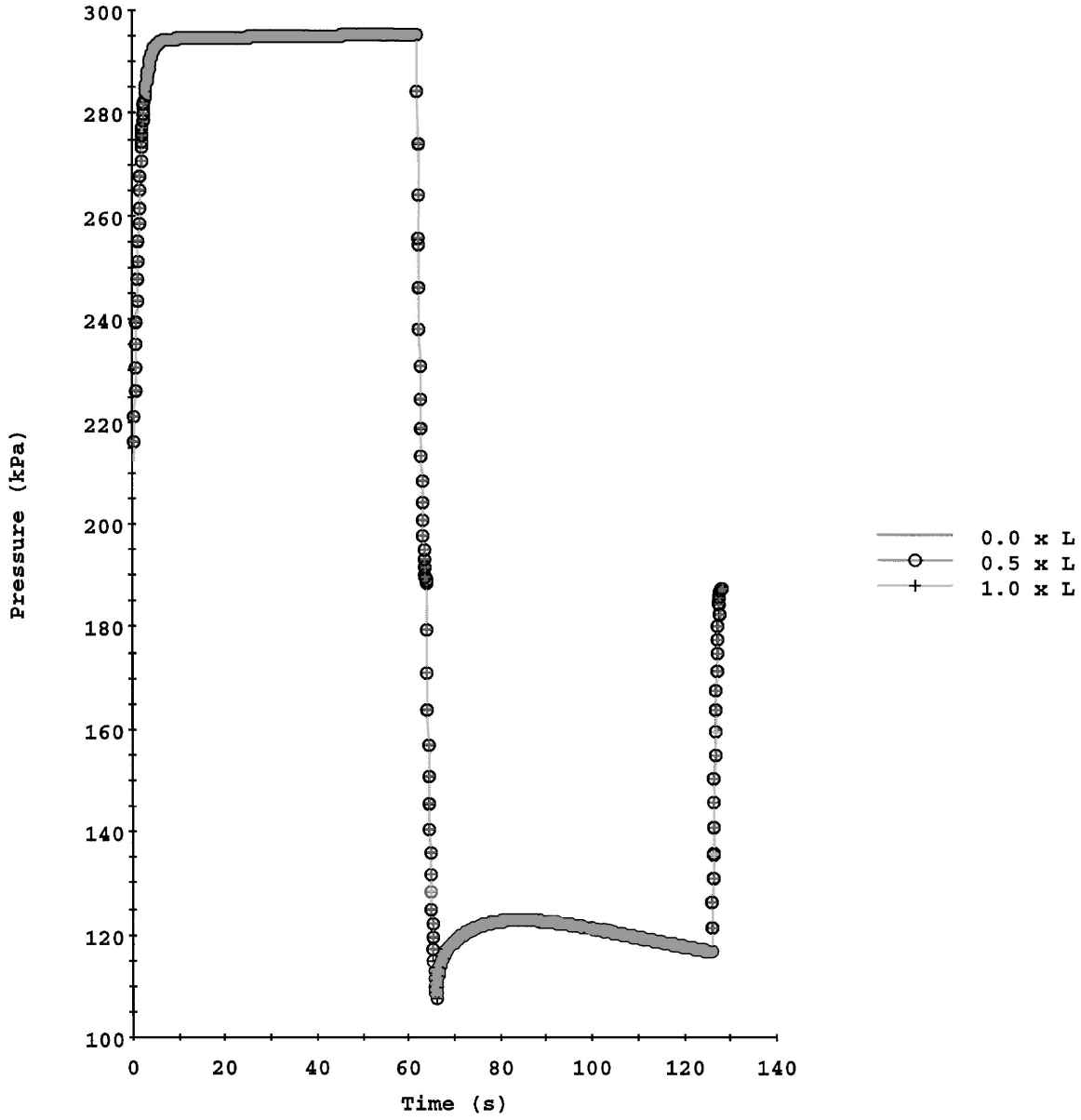

Figure 10. Pressure variation at base case conditions during cyclic steady state.

5.5. *Direct Cyclic Steady State Determination by Complete Discretisation*

We now attempt to determine the CSS directly via the complete discretisation approach of Section 3.2. An implementational complication arises in this context. This is caused by the fact that the adsorption and desorption steps are much longer than the other steps in the cycle for this process. On the other hand, the time-domain normalisation procedure described in Section 3.3.1 (see also Fig. 3) assigns equal importance to all steps in the cycle by reducing each one of them to a normalised length of 1.

The problem with the above situation is that applying a uniform discretisation grid to the *normalised* time domain will actually result in a much finer time discretisation for the four shorter steps in comparison to the two longer ones. To a certain extent, this is justified given the fact that time variations are normally much faster during the short pressure equalisation and

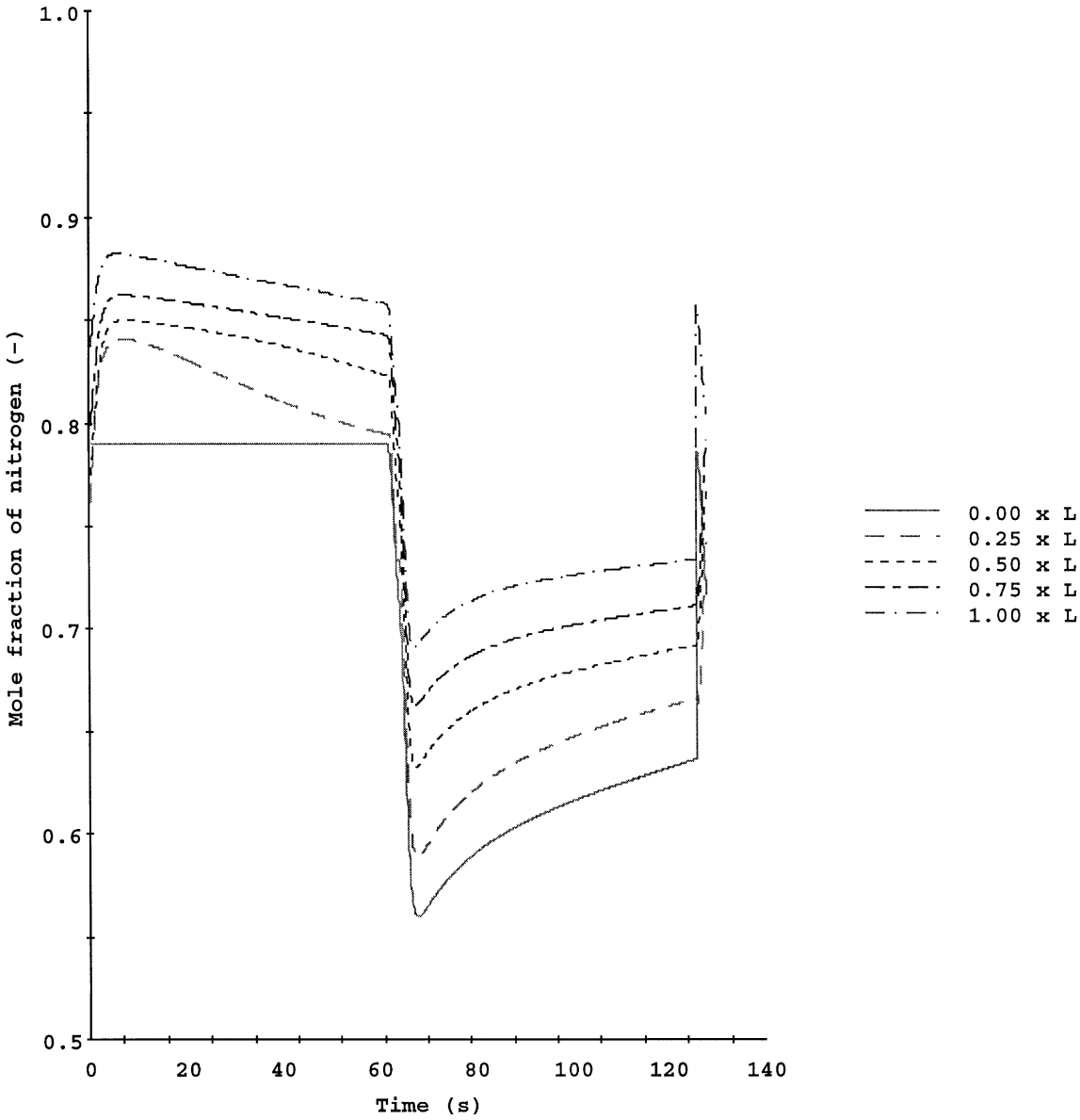

Figure 11. Nitrogen mole fraction variation at base case conditions during cyclic steady state.

blowdown steps. However, to achieve a more efficient utilisation of the time discretisation grid, we make the long steps four times longer than the short ones in the "normalised" time domain. This is illustrated in Fig. 13.

5.5.1. Comparative Results. Table 11 compares the values of various process performance measures predicted by the dynamic simulation and complete discretisation methods. The relative differences reported in this Table are computed according to Eq. (74). It can be seen that this is generally of the order of 2%.

Table 11. Dynamic simulation and complete discretisation results for modified Skarstrom cycle process at base case conditions.

Performance measure	[DS]	[CD]	% Rel. Difference
O_2 impurity (%)	12.91	12.90	−0.07
N_2 recovery (%)	69.91	67.45	−3.45
Production rate (mol s^{-1})	5.97×10^{-4}	5.84×10^{-4}	−2.18
Feed rate (mol s^{-1})	9.40×10^{-4}	9.55×10^{-4}	1.60
Average power requirement (W)	1.13	1.15	1.77

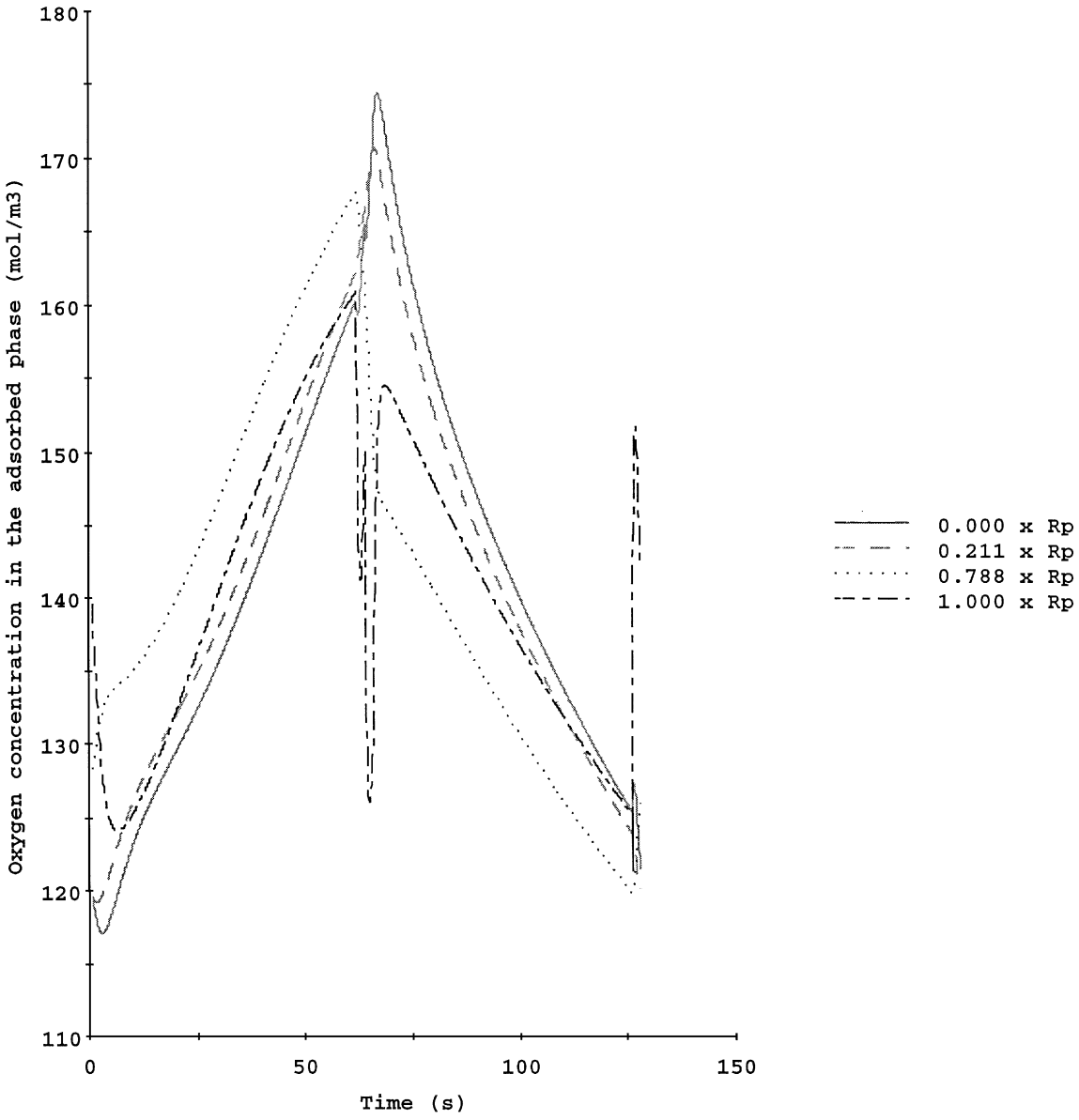

Figure 12. Adsorbed phase oxygen concentration variation at base case conditions at $z = \frac{L}{4}$ during cyclic steady state.

Figures 14 and 15 show more detailed comparisons of the dynamic simulation and complete discretisation results. Each figure displays 6 pairs of axial profiles of a different quantity. Each pair involves one axial profile computed using dynamic simulation and the corresponding one obtained using complete discretisation; both profiles are shown at the middle of each of the 6 operating steps of the cycle (cf., Section 5.1). More results of this type are given by Nilchan (1997).

The overall conclusion is that the complete discretisation approach is generally successful in predicting the behaviour of the process with reasonable accuracy. The largest discrepancies occur during the blowdown and pressure equalisation steps, during which the fastest temporal variations take place.

5.5.2. Numerical Efficiency Considerations. The complete discretisation approach results in a system of 15487 nonlinear algebraic equations with a Jacobian matrix with 96552 non-zero elements. The equations were solved using a Newton-type iterative method

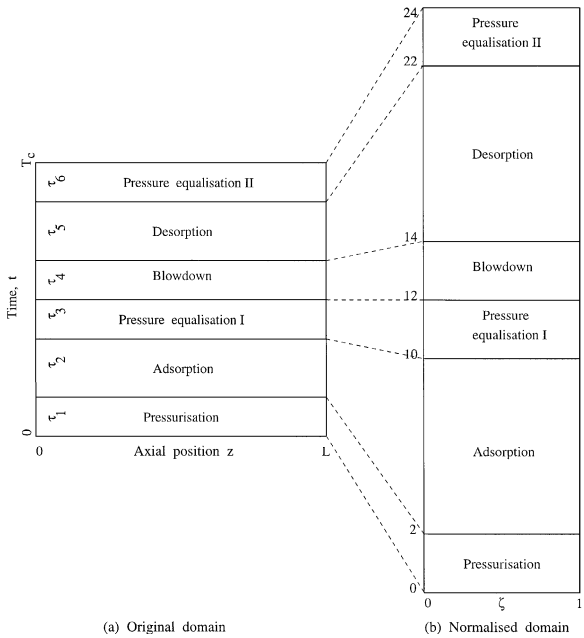

Figure 13. Normalisation of spatial/temporal domain for modified Skarstrom cycle process.

implemented in *gPROMS*; the iterations were initialised with all concentrations (in both the gas and solid phases) being set to 200 mol m^{-3}, all pressures to 3×10^5 Pa and all velocities to 0.1 m s^{-1}. The solution was obtained in 19 iterations.

The total CPU time required by the complete discretisation approach was 3700 seconds on a SUN UltraSPARC workstation. The corresponding CPU time for the dynamic simulation approach was 2600 seconds (for the 60 cycles required to reach CSS). Thus, for this process, the computation of a "one-off" CSS using the complete discretisation approach is more expensive than with the dynamic simulation one. However, the real advantage of the new approach lies in its improved efficiency for parametric studies (see comment at the end of Section 4.5.2), and also in its suitability as the basis for formal process optimisation.

5.6. *Optimisation of the Modified Skarstrom Cycle Process*

We now turn our attention to the optimisation of the modified Skarstrom cycle process. The optimisation decision variables are those listed in Table 9. We note that the duration of only one of the two pressure equalisation steps is an independent decision variable: the interactions between the two beds in the process constrain these two steps always to be of equal duration (cf., constraint (9)).

Table 12. Optimal decision variable values for the modified Skarstrom cycle process.

Decision variable	Units	Value
Feed pressure	bar	2.60
Bed length	m	0.5
Pressurisation time	s	5.74
Adsorption time	s	60.51
Pressure equalisation time	s	3.07
Blowdown time	s	10.0
Desorption time	s	30.0

The objective function to be minimised is the average power requirement (see Eq. (97)). The maximum acceptable oxygen impurity in the product stream is set at 12.9% and the minimum acceptable average production rate at 5.84 $\times 10^{-4}$ mol s^{-1}. These are the values predicted by the complete discretisation approach under base case conditions (see Table 11).

The optimisation run is performed by varying all seven decision variables simultaneously. The optimum is obtained within 6 optimisation iterations taking approximately 220 minutes of CPU time on a SUN UltraSPARC workstation. This computational time is only about 5 times higher than the time required to determine a single CSS using dynamic simulation.

The optimal values of the decision variables are shown in Table 12, and the values of key performance parameters in the third column of Table 13. By comparing these results with the corresponding base case values (last column of Table 9, and third column of Table 11 respectively), it can be seen that the optimisation has resulted in a 14.5% reduction in the average power requirement. Both the product purity and the product throughput constraints are satisfied by the optimal solution.

As in the case of the RPSA process, we seek to verify the results of the optimisation by carrying out a dynamic simulation over a sufficiently large number of cycles with all decision variables set at their optimal values. The comparative results obtained are shown in Table 13. It can be seen that the agreement between the prediction of the complete discretisation and the dynamic simulation approaches is good, and that the improvement in performance predicted by the optimisation is not the result of numerical discretisation error.

Table 13. Verification of optimisation results via dynamic simulation for the modified Skarstrom cycle process.

Performance measure	Units	Optimal values predicted by [CD]	Values calculated by [DS]	Relative difference (%)
O_2 impurity	%	12.89	12.99	−0.76
N_2 recovery	%	67.60	68.45	−1.24
Production rate	mol s^{-1}	5.84×10^{-4}	5.95×10^{-4}	−1.84
Feed rate	mol s^{-1}	9.52×10^{-4}	9.47×10^{-4}	0.52
Average power requirement	W	0.98	0.99	−1.01

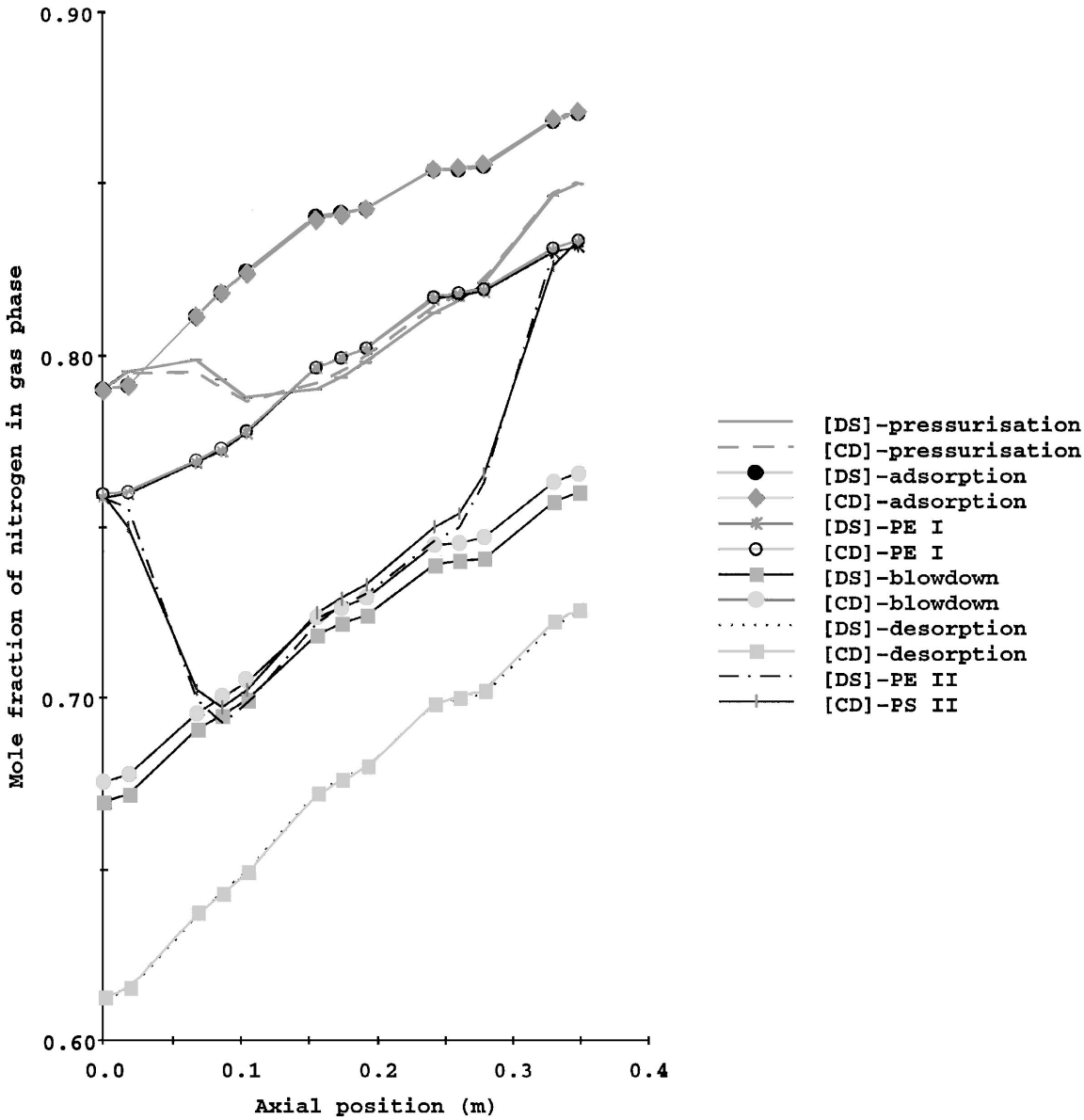

Figure 14. Base case nitrogen mole fractions in the gas phase obtained using dynamic simulation [DS] and complete discretisation [CD].

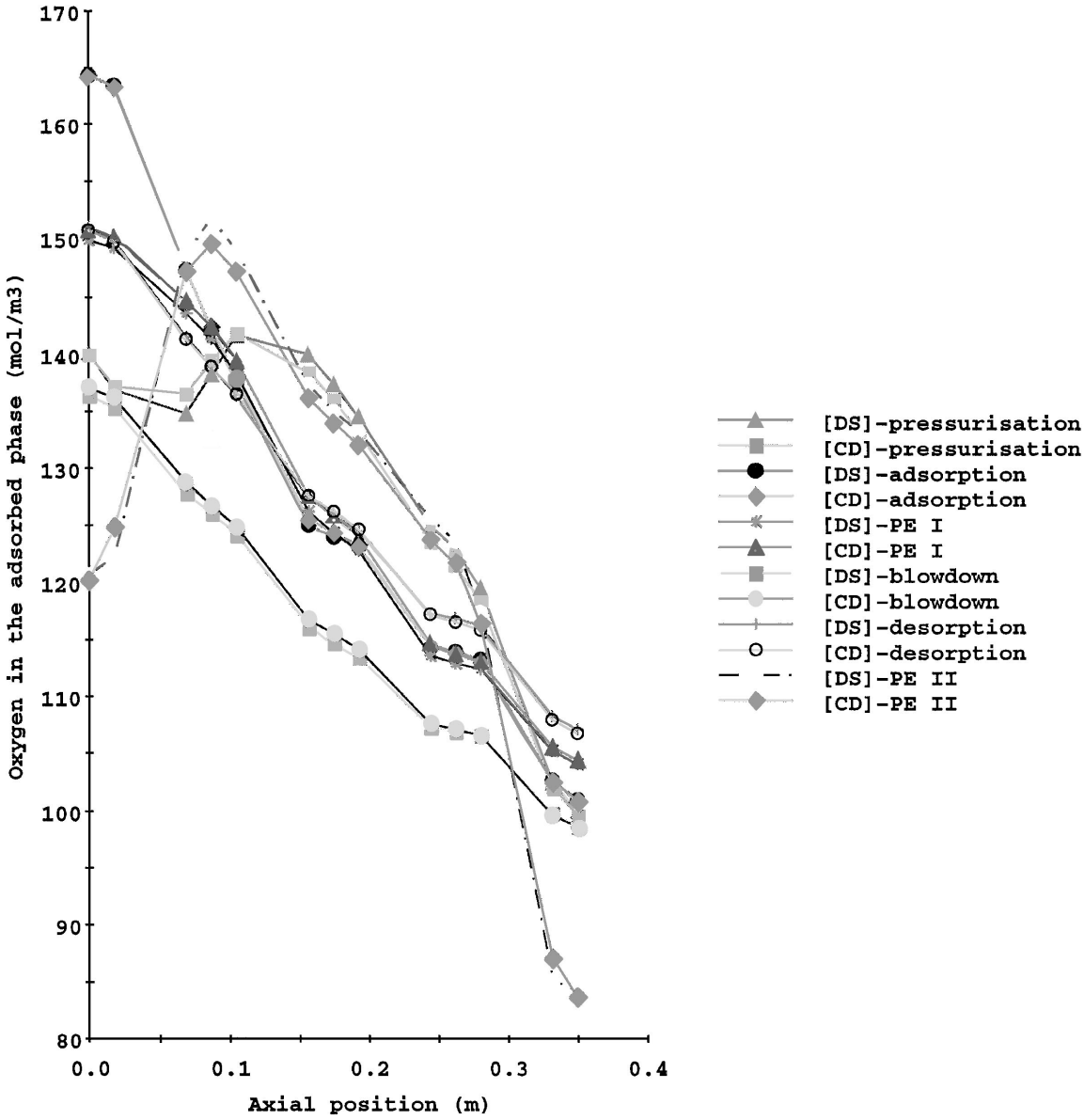

Figure 15. Base case oxygen concentration at the particle surface ($r = 0.003175$ m) obtained using dynamic simulation [DS] and complete discretisation [CD].

6. Concluding Remarks

This paper has presented a methodology for the optimisation of periodic adsorption processes operating at cyclic steady state conditions. The approach is based on a general mathematical formulation of the problem as a mixed set of partial differential and algebraic equations (PDAEs) subject to a set of spatial and temporal boundary conditions expressing the periodicity of the process and the interactions among the various beds in it. A variety of process performance constraints can also be formulated mathematically in this context. The objective function is generally a combination of the capital and operating costs of the process. The size of the formulation is independent of the number of beds in the process.

The numerical method proposed for the solution of the above optimisation problem employs simultaneous

discretisation of both spatial and temporal variations, which greatly facilitates the handling of the complex boundary conditions. The PDAE system and its boundary conditions are reduced to a set of nonlinear algebraic equations. The process performance constraints and the objective function can also be expressed as nonlinear algebraic functions of the same discretised variables.

Overall, this leads to a nonlinear programming problem (NLP) with a large number of variables and constraints, but a relatively small number of degrees of freedom. The NLP is therefore solved using a sequential quadratic programming algorithm operating in the reduced space of these decision variables. A Newton-type iteration is used to solve the discretised equations for any given set of values of the decision variables manipulated by the optimiser.

It is interesting to note that simultaneous spatial and temporal discretisation has been used before in the context of the simulation of periodic adsorption processes (see, for instance, Hassan et al., 1986; Alpay, 1992; Alpay et al., 1993). However, this was primarily viewed as an alternative to employing an integration algorithm for progressing time over a succession of individual cycles, rather than as a means for the direct determination and/or optimisation of the cyclic steady state.

Occasional mentions of the idea of directly imposing a periodic boundary condition in conjunction with a simultaneous spatial and temporal discretisation scheme have also appeared in earlier literature (see, for instance, Croft and LeVan, 1994a). However, to our knowledge, the mathematical and computational implications of this idea (e.g., with respect to handling interactions between multiple beds, or its optimisation extensions) have not been explored to any significant extent.

The work presented in this paper was primarily concerned with establishing the theoretical basis of the new approach. Thus, the solution methods used were completely generic, and no attempt was made to exploit the special structure of the underlying mathematical problem. Nevertheless, the examples presented demonstrate the overall feasibility of the approach when applied to processes of medium complexity described by fairly detailed models.

Finally, it should be noted that the main limitation of the proposed approach arises from the size of the system that is generated by the discretisation approach, and the trade-offs between this size and the accuracy of the results. The latter may be an issue especially when dealing with processes producing very high purity products. On the other hand, it should also be recognised that already it is possible to solve general sparse systems involving more than 200,000 nonlinear algebraic equations. Further improvements in the reliability and efficiency of numerical methods, and also the increasing availability of high performance computers will certainly widen the scope of problems that can be handled using our approach.

Acknowledgments

The authors wish to acknowledge the contribution of Ralph Schellen in preparing the initial version of the model used in Section 5 of this paper.

Notes

1. For instance, in the case of the equation of state mentioned above, we would treat it as one of the algebraic equation (3b) that are valid in the interior of the spatial domain, but we would also include it as one of the left and right boundary conditions (4) and (5) respectively.
2. Croft and LeVan (1994a, 1994b) consider single bed processes only.
3. One such model is presented in Section 5 for a modified Skarstrom cycle PSA process.
4. Note that the input variables U_{10} do not actually occur in the equations under consideration (cf. Eqs. (31) and (32)) and are therefore not included here.
5. In practice, $\Psi(\cdot)$ is likely to be a function of u only.

References

Alpay, E., Rapid Pressure Swing Adsorption Processes, Ph.D. thesis, University of Cambridge, 1992.

Alpay, E., C.N. Kenney, and D.M. Scott, "Simulation of Rapid Pressure Swing Adsorption and Reaction Processes," *Chem. Engng. Sci.*, **48**, 3173–3186 (1993).

Barton, P.I. and C.C. Pantelides, "Modeling of Combined Discrete/Continuous Processes," *AIChE J.*, **40**, 966–979 (1994).

Bird, R.B., W.E. Stewart, and E.N. Lightfoot, *Transport Phenomena*, John Wiley & Sons, New York, 1960.

Carey, G.F. and B.A. Finlayson, "Orthogonal Collocation on Finite Elements," *Chem. Engng. Sci.*, **30**, 587–596 (1975).

Carver, M.B., "Method of Lines Solution of Differential Equations—Fundamental Principles and Recent Extensions," *Foundations of Computer-Aided Process Design*, R.S.H. Mah and W.D. Seider (Eds.), Engineering Foundation, pp. 369–402, New York, New Hampshire, 1981.

Chou, C.T. and W.C. Huang, "Incorporation of a Valve Equation into the Simulation of a Pressure Swing Adsorption," *Chem. Engng. Sci.*, **49**, 75–84 (1994a).

Chou, C.T. and W.C. Huang, "Simulation of a Four-Bed Pressure Swing Adsorption Process for Oxygen Enrichment," *Ind. Engng. Chem. Res.*, **33**, 1250–1258 (1994b).

Croft, D.T. and M.G. LeVan, "Periodic States of Adsorption Cycles—I. Direct Determination and Stability," *Chem. Engng. Sci.*, **49**, 1821–1829 (1994a).

Croft, D.T. and M.G. LeVan, "Periodic States of Adsorption Cycles—II. Solution Space and Multiplicity," *Chem. Engng. Sci.*, **49**, 1831–1841 (1994b).

Farooq, S. and D.M. Ruthven, "Numerical Simulation of a Kinetically Controlled Pressure Swing Adsorption Bulk Separation Process Based on a Diffusional Model," *Chem. Engng. Sci.*, **46**, 2213–2224 (1991).

Finlayson, B.A., *Nonlinear Analysis in Chemical Engineering*, McGraw-Hill, New York, 1980.

Glueckauf, E. and J.I. Coates, "Theory of Chromatography: Part IV. The Influence of Incomplete Equilibrium on the Front Boundary of Chromatograms and on the Effectiveness of Separation," *J. Chem. Soc.*, 1315 (1947).

Habgood, H.W., "The Kinetics of Molecular Sieve Action. Sorption of Nitrogen, Methane Mixtures by Linde Molecular Sieve 4A," *Can. J. Chem.*, **36**, 1384–1397 (1958).

Hassan, M.M., D.M. Ruthven, and N.S. Raghavan, "Air Separation by Pressure Swing Adsorption on a Carbon Molecular Sieve," *Chem. Engng. Sci.*, **41**, 1333–1343 (1986).

Hassan, M.M., N.S. Raghavan, and D.M. Ruthven, "Pressure Swing Air Separation on a Carbon Molecular Sieve—II. Investigation of a Modified Cycle with Pressure Equalization and No Purge," *Chem. Engng. Sci.*, **42**, 2037–2043 (1987).

Jarvis, R.B. and C.C. Pantelides, "DASOLV—a Differential-Algebraic Equation Solver," Technical report, Centre for Process Systems Engineering, Imperial College, 1992.

Jones, R.L. and G.E. Keller, "Pressure Swing Parametric Pumping—A New Adsorption Process," *J. Sep. Proc. Tech.*, **2**, 17–23 (1981).

Kowler, D.E. and R.H. Kadlec, "The Optimal Control of a Periodic Adsorber," *AIChE J.*, **18**, 1207–1219 (1972).

Kvamsdal, H.M., Studies on Modeling, Simulation and Optimization of PSA Systems, Ph.D. thesis, University of Trondheim, 1995.

McCabe, W.L., J.C. Smith, and P. Harriott, *Unit Operations of Chemical Engineering*, McGraw-Hill, 4th edition, 1985.

Nilchan, S., On the Optimisation of Periodic Adsorption Processes, Ph.D. thesis, University of London, 1997.

Oh, M., Modelling and Simulation of Combined Lumped and Distributed Processes, Ph.D. thesis, University of London, 1995.

Oh, M. and C.C. Pantelides, "A Modelling and Simulation Language for Combined Lumped and Distributed Parameter Systems," *Comp. chem. Engng.*, **20**, 611–633 (1996).

Paloschi, J.R., The Numerical Solution of Nonlinear Equations Representing Chemical Processes, Ph.D. thesis, University of London, 1982.

Pritchard, C.L. and G.K. Simpson, "Design of an Oxygen Concentrator Using the Rapid Pressure-Swing Adsorption Principle," *Chem. Engng. Res. Des.*, **64**, 467–472 (1986).

Round, G.F., H.W. Habgood, and R. Newton, "A Numerical Analysis of Surface Diffusion in a Binary Adsorbed Phase," *Separation Sci.*, **1**, 219–244 (1966).

Ruthven, D.M., *Principles of Adsorption and Adsorption Processes*, John Wiley & Sons, New York, 1984.

Schiesser, W.E., *The Numerical Method of Lines*, Academic Press, New York, 1991.

Skarstrom, C.W., U.S. Patent No. 2,944,627, to Exxon Research and Engineering, 1960.

Smith IV, O.J. and A.W. Westerberg, "The Optimal Design of Pressure Swing Adsorption Systems," *Chem. Engng. Sci.*, **46**, 2967–2976 (1991).

Turnock, P.H. and R.H. Kadlec, "Separation of Nitrogen and Methane via Periodic Adsorption," *AIChE J.*, **17**, 335–342 (1971).